Strike-slip deformation reflects complex partitioning of strain in the Nankai Accretionary Prism (SE Japan)

Marco C. Azevedo [a], Tiago M. Alves [a], Paulo E. Fonseca [b], and Gregory F. Moore [c]

[a] *3D Seismic Lab, School of Earth and Ocean Sciences, Cardiff University, Main Building, Park Place, CF10 3AT Cardiff, United Kingdom*

[b] *Departamento de Geologia, and Instituto Dom Luiz Faculdade de Ciências, Universidade de Lisboa, 1749-016 Lisboa, Portugal*

[c] *Department of Geology and Geophysics, University of Hawaii, 1680 East-West Rd., Honolulu, HI 96822, United States*

ABSTRACT

Previous studies have suggested predominant extensional tectonics acting, at present, on the Nankai Accretionary Prism (NAP), and following a parallel direction to the convergence vector between the Philippine Sea and Amur Plates. However, a complex set of thrusts, pop-up structures, thrust anticlines and strike-slip faults is observed on seismic data in the outer wedge of the NAP, hinting at a complex strain distribution across SE Japan. Three-dimensional (3D) seismic data reveal three main families of faults: (1) NE-trending thrusts and back-thrusts; (2) NNW- to N-trending left-lateral strike-slip faults; and (3) WNW-trending to E-W right-lateral strike-slip faults. Such a fault pattern suggests that lateral slip, together with thrusting, are the two major styles of deformation operating in the outer wedge of the NAP. Both styles of deformation reflect a transpressional tectonic regime in which the maximum horizontal stress is geometrically close to the convergence vector. This work is relevant because it shows a progressive change from faults trending perpendicularly to the convergence vector, to a broader partitioning of strain in the form of thrusts and conjugate strike-slip faults. We suggest that similar families of faults exist within the inner wedge of the NAP, below the Kumano Basin, and control stress accumulation and strain accommodation in this latter region.

Keywords: Convergent margins; SE Japan; accretionary prism; strike-slip; transpression.

1. INTRODUCTION

The Nankai Trough is one of the most studied subduction zones in the world and delineates an active, seismogenic convergent margin under which the Philippine Sea Plate is being subducted under the Amur Plate at a variable rate of 2 to 6.5 cm/year (Miyazaki and Heki, 2001; Tsuji et al., 2014). Recent work identified a dominantly compressional area of the accretionary prism, controlled by a large "Megasplay Fault Zone" (MSFZ), on the upper continental slope of the Nankai Trough (Moore et al., 2007; Kimura et al., 2011; Moore et al., 2015). In the published literature, the MSFZ is associated with a WNW- directed (~ N120°–N125°) convergence vector that is deviated ~ 15°- 45° counter-clockwise from a direction orthogonal to the trench (e.g. DeMets et al., 2010; Tsuji et al., 2014).

Submarine accretionary prisms and associated structures are usually described by the classical critical-wedge and dynamic Coulomb-wedge theories (Davis et al., 1983; Dahlen et al., 1984), with the Nankai Accretionary Prism (NAP) being no exception (Wang and Hu, 2006). These two theories suggest a transition between a highly compressional outer wedge and a less compressional and moderately seismogenic inner wedge. As a result, Wang and Hu (2006) described the outer wedge of the NAP as comprising a series of imbricate thrust faults (i.e. reflecting a zone of low shear strength), while the inner wedge forms a zone of accreted sediment, normally acting as a backstop. The inner wedge of the NAP is characterized by the absence of active compressional structures. Reference to important strike-slip movements in the landward part of the MSFZ was made by Martin et al. (2010) and Tsuji et al. (2014), who justified these movements as reflecting a transtensional tectonic regime. Such a regime allowed the formation of small to regional-scale trench-parallel and right-lateral strike-slip faults with associated normal offsets. The same authors stated that present-day transtension is associated with oblique subduction at obliquity values as little as 15°. However, Byrne et al. (1993) also stated that a detailed picture of an underlying backstop could not be determined from surface information alone.

The theoretical interpretation of a predominantly compressional accretionary prism offshore Nankai was developed further by Byrne et al. (2009), Moore et al. (2013) and Lin et al. (2015), who confirmed the existence of a component of extension acting near the sea floor. In fact, extensional tectonics accounts for most of the modern deformation recorded in the forearc basin that overlies the inner wedge of the NAP. According to Wang and Hu (2006), Byrne et al. (2009) and Lin et al. (2015), this extensional regime is particularly active during inter- seismic cycles. Nevertheless, Lin et al. (2015) show evidence for compression at Integrated Ocean Drilling Program (IODP) Sites C0004 and C0010, seaward from the MSFZ, with a $\sigma 1$ parallel to the convergence vector. Alternative interpretations consider stress decoupling between a shallow regime of normal faulting and a deeper regime of strike-slip faulting and thrusting in both the inner and outer wedges of the NAP (Moore et al., 2013; Van Tuyl et al., 2015).

Previous reference to strike-slip faults and flower structures in the outer wedge of the northeast NAP (Zenisu area) was made by Le Pichon et al. (1992; 1996). In the Nankai Trough region, flower structures and associated strike-slip faults were identified by Takahashi et al. (2002). In parallel, microseismicity studies documented the rupture of a major NW-trending, right-lateral strike-slip fault crossing the outer wedge of the NAP during the 2004 earthquake off the Kii Peninsula (M = 7.4) (Obana et al., 2005). Obana et al. (2005) proved the existence of several N- to NE-trending strike-slip fault systems operating within the Shikoku Basin. Similar strike-slip faults in the seaward part of the MSFZ, and outer wedge of NAP, have been interpreted as inherited structures from the subducted crust (Shikoku Basin) (Kodaira et al., 2006). Moore et al. (2013, 2015) focused on the Kumano Basin, which overlies the inner wedge of the NAP, to interpret two major WNW-trending strike-slip faults offsetting both the outer wedge of the NAP and the MSFZ. Not-withstanding all this work, most of recent research has been focused on the landward (Kumano Basin) and most seaward (Frontal Thrust Zone) parts of the NAP, where in-situ stresses measured at several IODP Sites have demonstrated that extension predominates at present (Lin et al., 2015).

In order to understand the structural evolution of the outer wedge of the NAP and, ultimately, of the NAP itself, it is necessary to assess: (1) where and how tectonic stresses accumulate in the prism, and (2) how shallow and deep structures relate across distinct sub-surface units. Strike-slip faulting that is not associated with the MSFZ, and within the outer wedge of the NAP, was mentioned in previous work but never fully characterized or studied, resulting in a relative under-re- presentation of this tectonic regime in the published literature. The outer wedge is considered to be the zone most actively deforming in accretionary prisms, and where the response to tectonic stresses is better expressed (MacKay et al., 1992; Park et al., 1999). Several questions remain to be addressed, some of which will have a large impact on the present understanding of NAP's tectono-stratigraphic evolution. Hence, the key aims of this work are:

1. To describe the structural framework of the outer wedge of the NAP;

2. To investigate the tectonic regime operating in the outer wedge of the NAP, as well as its related stress field(s), based on structural analyses of 3D seismic data;

3. To compare and discuss our interpretations with published information on the inner wedge of the NAP and older accretionary prisms.

2. REGIONAL GEOLOGICAL SETTING

2.1 Stress field and associated deformation styles

Knowledge on the stress state(s) at accretionary prisms is of paramount importance to assess how strain is accommodated inside them and, subsequently, to determine their deformation style(s). Taking into account that the study area is divided in an inner and outer wedge, with a transitional area that is mainly controlled by the MSFZ (Wang and Hu, 2006; Kimura et al., 2011), we follow the dynamic wedge theory of Wang and Hu

(2006) to individualize the stress states in the NAP. We use this latter theory, instead of the classic wedge concepts in Davis et al. (1983), as this latter is known to generalize the stress states for the study area.

According to Wang and Hu (2006), the mechanics of the inner and outer wedges of the NAP are different due to the distinct behavior of their décollement, or subduction fault. In the inner part of the wedge, the décollement has a velocity weakening behavior (downdip zone) that locks it, allowing stress to accumulate until a critical point, leading to its rupture. It thus comprises a seismogenic zone. However, the inner wedge rarely ruptures compressively due to its relatively low basal friction, a character allowing for significant slip along its décollement. This means the décollement does not lock in the entire section of the NAP. In the outer wedge of the NAP (updip zone), the décollement has a velocity strengthening behavior that does allow stress to build up to a critical state, and generates a highly compressional region at the toe of the continental slope (Fig. 2A and B).

Wang and Hu (2006) argue that wedge mechanics also varies with the seismic cycle due to changes in the stress state during and after an earthquake. During an earthquake, $\sigma 1$ is subhorizontal and the décollement slips, pressurizing the outer wedge into elastic or permanent compressive deformation. In contrast, the inner wedge is in a stable extensional state, as shear stress is null due to slip in the décollement. After an earthquake, the outer wedge records interseismic relaxation that is accompanied by a decrease in shear stress, seaward movement of this part of the NAP, and an increase in the dip of $\sigma 1$, whereas the inner wedge starts to become more compressional as shear stresses start to build up again.

Several methods have been applied to IODP data to define the stress field and deformation style(s) currently operating across the NAP, and on the incoming Philippine Sea Plate (Shikoku Basin) (Wu et al., 2013; Lin et al., 2015; Huffman and Saffer, 2016; Chang and Song, 2016). These papers not only show important changes in the stress field and deformation style(s) across the NAP, and between the NAP and Shikoku Basin; they also show results that are not consistent for the same IODP sites. This is due to the fact that different methods

have been applied to define these stress field(s) and associated deformation regime(s), and that measurements were taken at different depths and scales of observation.

Wu et al. (2013) used a compilation of Formation Micro Imager (FMI), Logging While Drilling (LWD) and core data to calculate the magnitudes of maximum (σ_{Hmax}) and minimum (σ_{hmin}) horizontal stresses. The magnitudes were constrained in stress polygons to derive the field stress in different areas of the NAP and Shikoku Basin. At IODP Site C0009, in the inner wedge of the NAP and at ~1540 metres below sea floor (mbsf), Wu et al. (2013) showed that σ_{Hmax} and σ_{hmin} correspond to σ_1 (maximum stress) and σ_3 (minimum stress), respectively. Here, $\sigma 1$ is perpendicular to the trench direction (which is NE-trending), and the deformation style is strike-slip faulting. However at IODP Site C0002, in the seaward part of the inner wedge (at ~ 1000 mbsf), the same authors estimated a NE-trending σ_{Hmax} where $\sigma_v > \sigma_{Hmax}$, a configuration that reflects a normal faulting regime. At IODP Site C0006, in the Frontal Thrust Zone (~476 mbsf), Wu et al. (2013) interpreted a normal faulting regime with a vertical σ_1 (σ_v), but close to strike-slip faulting due to σ_{Hmax} being NW-trending and only 0.5 MPa lower than σ_v. In the Shikoku Basin, at IODP Site C0011 (~610 mbsf), the stress field and deformation styles are similar to IODP Site C0002, but again very close to strike-slip faulting due to the minor difference in magnitude between σ_v and σ_{Hmax}. Despite these results, Wu et al. (2013) state that their stress analysis was limited by the total drilling depth, borehole conditions and deviations in the slip deficit method, thus returning less reliable results at relevant depths.

Lin et al. (2015) used a similar approach to Wu et al. (2013) in a larger number of IODP Sites across the NAP and Shikoku Basin, together with hydraulic fracturing experiments and anelastic strain recovery (ASR) measurements on retrieved cores. This approach allowed a detailed investigation of stress states across the NAP and Shikoku Basin, in three dimensions, leading to the conclusion that, overall, the NAP is currently undergoing a (inter-seismic) extensional regime.

136 According to Lin et al. (2015), the sediment cover overlying the inner wedge of the NAP (Kumano Basin)
137 has a vertical σ_1 and expresses a normal faulting regime. However, the strikes of σ_{Hmax} at IODP Sites C0009
138 and C0002 agree with the results in Wu et al. (2013). The transition from the Kumano Basin strata to the
139 inner wedge of the NAP is accompanied by a change in σ_1 from vertical to sub-horizontal, where $\sigma_{Hmax} = \sigma_1$,
140 and by a change from normal to strike-slip and thrust faulting. At the MSFZ, IODP Site C0001 shows a
141 similar stress distribution (and deformation style) to that of IODP Site C0009 with depth, with the change
142 occurring at ~500 mbsf. However, at IODP Sites C0004 and C0010, where the hanging-wall of the MSFZ
143 was drilled, σ_1 is interpreted to be sub-horizontal and parallel to the plate convergence vector, reflecting
144 thrust and strike-slip faulting regimes. In the shallower part of the hanging-wall of the Frontal Thrust Zone,
145 drilled at IODP Sites C0006 and C0007, Lin et al. (2015) interpreted a similar stress field and deformation
146 style to the shallow part of IODP Site C0001. Finally, in the Shikoku Basin, the interpretation of IODP Site
147 C0011 coincides with the results in Wu et al. (2013), while at IODP Site C0012 ASR analyses show evidence
148 for strike-slip and reverse faulting with a NE-trending σ_{Hmax}. In such a setting, Lin et al. (2015) state that, at
149 present, the overall NAP is dominated by a shallow ex- tensional regime and a relatively deep strike-slip to
150 reverse faulting regime, mainly due to stress field reorganization in the areas where $\sigma 1$ becomes σ_{Hmax}. This
151 transition between different tectonic regimes at depth is often referred to as Extension-Compression Depth
152 (ECD) and there is consistent data suggesting that the ECD is highly variable along the entire NAP, in both
153 the inner and outer wedges, depending on the thickness of the overlying sediment cover (Lewis et al., 2013;
154 Van Tuyl et al., 2015; Lin et al., 2015). Lin et al. (2015) refer that principal stresses permute in the deeper
155 levels of the NAP, but that sediment cores have yet to be recovered at such depths.

156 Recently, Chang and Song (2016) integrated borehole breakouts, drilling-induced tensile fractures and leak-
157 off tests at IODP Site C0002 to interpret tectonic stresses (up to a depth of ~2000 mbsf) at the seaward limit
158 of the inner wedge of the NAP. They concluded that deformation in this latter region varies between strike-
159 slip and normal faulting as a result of σ_{Hmax} and σ_v having similar magnitudes. They stress that σ_{Hmax} is NE-

160 trending above the MSFZ. The same authors postulate that strike-slip and extensional structures are found in
161 both core and regional seismic data.

162 In the Muroto Transect, outside our study area but still in the NAP, Huffman and Saffer (2016) showed
163 similar results and interpretations to the authors previously mentioned. Stress states at the toe of NAP are
164 likely associated with strike-slip or thrust faults across the active Frontal Thrust Zone down to a depth of
165 ~800 mbsf. The uppermost 300 mbsf are near thrust failure, where $\sigma_{Hmax} > \sigma_v$. However, Huffman and Saffer
166 (2016) conclude that the stress state in the upper 300 mbsf changes into a normal faulting regime at depth,
167 where $\sigma_v > \sigma_{Hmax}$. These authors recognize the large uncertainties associated with the parameters used in their
168 stress analysis.

169 It is important to highlight that limitations such as the depth and location of the boreholes, and conditions in
170 which data were acquired, can influence the analysis of regional stress states. Nevertheless, there seems to be
171 an overall consensus that the NAP is a compressional structure currently dominated by shallow normal (Wu
172 et al., 2013; Lin et al., 2015; Chang and Song, 2016) and strike-slip (Huffman and Saffer, 2016; Chang and
173 Song, 2016) faulting regimes. Borehole data are clear that shallower stress conditions differ from those
174 affecting deeper strata, but the lack of deep measurements does not allow definite conclusions about the
175 stress field and deformation styles operating at depth, and on the relationship between the shallow and deep
176 settings of the NAP. Furthermore, it is clear that strike-slip is an important deformation style within the NAP
177 that is yet to be characterized in detail.

178 Against this backdrop, three-dimensional interpretations of stress magnitudes and tensors along the NAP are
179 not unequivocal at some drilling sites. Furthermore, stress field studies have not been performed in the outer
180 wedge of the NAP due to the lack of borehole data in this region, and at higher depths within the inner wedge
181 (below the sediment cover of the Kumano Basin). This means that extrapolations based on few localized
182 wells in the MSFZ and inner wedge are not fully reliable, and a detailed analysis of 3D pre-stack depth

183 migration (PSDM) seismic data from the outer wedge of the NAP can be crucial to understand its structural
184 and stress evolutions.

185

186 **2.2 Seismic stratigraphy**

187 Most lithological information acquired in the NAP derives from core and well-log data gathered by the
188 NanTroSeize Project. IODP Sites C0018A (Figs. 1, 2B and C) and C0006 (Fig. 1A), which are respectively
189 located seaward of the MSFZ (in the outer wedge of the NAP) and in the Frontal Thrust Zone, provide
190 valuable lithological and stratigraphic information on the shallow sedimentary cover, uppermost part of the
191 accretionary prism, and underthrusted sediments from the Philippine Sea Plate. Multiple IODP campaigns
192 reached strata within the outer wedge of the NAP, and collected stratigraphic evidence to show that the study
193 area is mainly composed of a relatively thin Unit I (Expedition 315 Scientists, 2009; Expedition 316
194 Scientists, 2009; Kimura et al., 2011; Strasser et al., 2014). Slope sediments were accumulated above an
195 angular unconformity separating them from an underlying Unit II, this latter comprising strata belonging to
196 the upper part of the accretionary prism (Kimura et al., 2011) (Fig. 2D). In addition, cores collected at IODP
197 Site C0006 drilled through a deep Unit III composed of underthrusted deep-marine sediment from the
198 subducting Shikoku Basin.

199 Unit I can be up to 2.4 Ma old and comprises slope-apron fine- grained turbidite facies spanning the latest
200 Pliocene-Holocene. Data from IODP Sites C0008 and C0018A (Expedition 315 Scientists, 2009; Expedition
201 316 Scientists, 2009; Expedition 333 Scientists, 2012) di- vided Unit I into Units Ia, Ib and Ic, which mark a
202 gradual transition from upper-slope apron facies to base of slope apron facies. Unit Ia comprises hemipelagic
203 mud and silty-clay sequences intercalated with multiple ash layers. Unit Ib is composed of hemipelagic mud,
204 silty clay and silty turbidites with ash layers. Finally, Unit Ic reflects sediment deposited above Unit II and it

205 is characterized by turbiditic sand and sandy silt intercalated with mud and ash layers (Expedition 315
206 Scientists, 2009; Kimura et al., 2011; Alves et al., 2013; Strasser et al., 2014).

207 IODP Sites C0006, C0008 and C0018 (Expedition 315 Scientists, 2009; Expedition 316 Scientists, 2009)
208 define Unit II as reflecting the uppermost part of the accretionary prism. This unit is considered to be
209 Pliocene in age or older (Expedition 315 Scientists, 2009; Expedition 316 Scientists, 2009; Alves et al.,
210 2013). It comprises accreted sediments with mudstone- to sand-dominated lithologies (Expedition 315
211 Scientists, 2009; Kimura et al., 2011; Alves et al., 2013; Strasser et al., 2014).

212 Unit III was identified below Unit II in the Frontal Thrust Zone, at IODP Sites C0006 and C0007 (Expedition
213 316 Scientists, 2009), and comprises hemipelagic mud interbedded with volcanic ash and tuffs. Unit III is
214 deformed by thrust faults and transitions at depth into Unit IV, which represents underthrusted Shikoku Basin
215 sediment (Expedition 316 Scientists, 2009).

216 In the inner wedge of the NAP, the presence of an overlying forearc basin (Kumano Basin), and underlying
217 thrust-and-fold accretionary prism, agrees with the stratigraphic units defined by IODP Expeditions 315 and
218 316. However, slope sediments are relatively thin and dis- continuous in the outer wedge of the NAP, having
219 been removed by erosion at places (Van Tuyl et al., 2015). This means that Unit I may not exist in most of
220 the outer wedge. Furthermore, it is difficult to characterize the strata inside the outer wedge of the NAP due
221 to the lack of borehole data crossing the complex, folded sequences that form this same prism. In the study
222 area, 3D seismic data show that the accretionary prism should be divided in several tectono-stratigraphic
223 units instead of being classified as Unit II and Unit III (Fig. 2B).

224 As the focus of this work is the structural interpretation of the outer wedge of the NAP, we used published
225 information on Unit I (due to the extensive core/log data acquired in this latter) to propose an adaptation of
226 the tectono-stratigraphic division of the outer wedge of the NAP in Park et al. (2010). In our work, the upper
227 part of Unit A comprises the overthrusting package that includes Unit II. Unit B is the Low Velocity Zone

(LVZ) identified by Park et al. (2010) and Kamei et al. (2012). Unit C is the underthrusting part of the accretionary prism (Figs. 2A and B). The deepest unit in the study area corresponds to subducted oceanic crust in which seismic resolution is significantly lower. Based on Park et al. (2010), Unit C represents underthrusted sediments that under- plate Unit A as defined in this work, while maintaining a critical taper in the modern accretionary prism. This geometry allows the seaward growth of Unit A to produce the LVZ and associated Unit B. In contrast, Kamei et al. (2012) propose a thicker LVZ that includes both Units B and C from Park et al. (2010), with a décollement on top of Unit C.

The seismic data used in this work show clear evidence for two units of low reflectivity separated by a strong seismic reflection (décollement), strengthening the idea that Units B and C represent similar lithologies, i.e. Unit B originating from the underthrusting or underplating of Unit C (Bangs et al., 2009; Park et al., 2010; Kamei et al., 2012). Bangs et al. (2009) discussed the possibility of the décollement being initially at the top of the LZV (Unit B), changing later to its present-day position. Such a character suggests a similar lithology across Units B and C, but with both units reflecting distinct tectonic and rheological behaviors.

3. STUDY AREA AND METHODOLOGY

The study area is located in the southeast coast of Japan, just off the Kii Peninsula, within what is known as the Kumano Transect (Fig. 1A). In this transect, a 3D pre-stack depth migrated (PSDM) seismic volume was acquired across the Nankai continental slope as part of the Nankai Trough Seismogenic Zone Experiment (NanTroSEIZE) (Figs. 1B and 1C). The study area comprises the southern half of the acquired 3D PSDM seismic block, imaging the Imbricate Thrust and Frontal Thrust Zones just seaward of the MSFZ (Moore et al., 2001; Park et al., 2002; Tobin and Kinoshita, 2006) (Fig. 1B-C). This region is also known as the outer wedge of the NAP.

250 Mapping and interpretation of seismic horizons, complemented by the compilation of attribute maps, form
251 the basis of our structural analysis (Figs. 2 and 3). The interpreted seismic volume has an inline spacing of
252 12.5 m, a crossline spacing of 18.75 m, and was acquired using a 2-source array with four receiver cables at a
253 distance of 150 m. Each receiver cable was 4500 m long, with 360 receiver groups spaced 12.5 m, and was
254 able to acquire nominal 60-fold data. Data processing included pre-stack multiple removal and data
255 conditioning (e.g., amplitude recovery, time-variant filtering, and predictive deconvolution) followed by 3D
256 pre-stack depth migration (Moore et al., 2009). Seismic resolution can reach < 5 m at the depth of the
257 shallower faults in this paper, for a range of 6–10 m in the deeper strata based on the dominant wavelength of
258 ~24 m observed on synthetic logs and seismic profiles. The main limitation of this method results from the
259 fact that it is only possible to observe, map and interpret structures that are within this latter range in seismic
260 resolution.

261 According to Roberts (2001) and Chopra and Marfurt (2005, 2007a, 2007b), attribute data such as coherence
262 and curvature have crucial importance to the 3D interpretation of seismic data. Both attributes are
263 particularly helpful in structural analyses, as they enhance faults that are often not recognized on vertical
264 seismic profiles or time-structure maps alone. Volumetric curvature is a property that measures lateral
265 changes in dip-magnitude and dip-azimuth waveforms (Mai et al., 2009). The presence of fractures and small
266 faults is closely related to reflection curvature. In this work, maximum curvature is used to visualize small-
267 scale faults and later obtain measurements of maximum horizontal displacements from them. In addition,
268 coherence comprises a technique cross-correlating seismic amplitudes in adjacent traces, and has a proven
269 record of efficiently portraying faults by measuring lateral changes in waveform (Chopra and Marfurt, 2005;
270 Mai et al., 2009). These attributes are automatically extracted from specialized seismic interpretation
271 software, such as Schlumberger's Petrel® used in this work, but it is necessary to choose a horizontal time- or
272 depth-slice that is deep enough to intersect a wide range of well-resolved structures. After careful

273 interpretation of the 3D PSDM seismic volume, we selected an area that had been significantly affected by
274 thrust-and-fold structures at a depth of 3840 m.

275 In this work, we classify the interpreted faults based on their strikes as there is a direct relationship between
276 their geometry and the observed deformation styles in the outer wedge of the NAP. Strike measurements are
277 automatically undertaken by the seismic interpretation software after faults are mapped. For curved faults and
278 fractures one measurement is taken as the average strike, which coincides with the best fitting straight line to
279 the curve. Taking into consideration that several authors agree with the interpretation of distinct deformation
280 regimes at shallow and deep levels of the NAP (e.g. Lin et al., 2015; Van Tuyl et al., 2015; Chang and Song,
281 2016), a classification based on the length of imaged faults, and their depth, can also be used. However, such
282 a classification will bear no relation to either the geometry or the deformation styles of such structures, as the
283 boundary between shallow and deep structures occurs at a variable depth.

284 Van Tuyl et al. (2015) explain that the depth of the ECD surface on 3D seismic data is markedly variable,
285 being shallower in the outer wedge than in the inner wedge, and clearly related to the thickness of overlying
286 slope sediment (Unit I). Therefore, in order to classify the different families of faults in terms of length and
287 depth they reached, we consider shallow structures as affecting the uppermost part of the NAP (Units A and
288 B), and deep structures as those propagating from the décollement, intersecting the décollement, or offseting
289 Unit C and oceanic crust.

290 Seismic attribute mapping provides the basis for statistical analyses of geometry, kinematics and dynamics of
291 the main faults in this work (Fig. 3). The strikes of thrusts and conjugate sets of strike-slip faults were
292 measured prior to the estimate of stress and paleostress fields from dihedral angles (Hancock, 1985). This
293 latter estimate provided the basis for our structural analysis, allowing the 3D mapping of small- and large-
294 scale faults and fractures, and detailed descriptions of their geometry, kinematics and dynamics. Our

approach included the quantitative characterization of faults' strike and their throws and horizontal (strike-slip) displacements, together with quatitative analyses of fault dips.

4. STRUCTURAL ANALYSIS

The Imbricate Thrust and Frontal Thrust Zones chiefly comprise NE- striking thrusts formed by horizontal shortening, dipping to the NW (in- sequence) or SE (out-of-sequence and back-thrusts) (see Moore et al., 2001; Gulick et al., 2004; Strasser et al., 2011). Nevertheless, seismic attribute maps reveal the existence of at least two more families of faults with conjugate geometries; a first trending WNW to E-W and a second trending N to NNW (Fig. 3). Two major NW-trending faults, belonging to the first of the two fault families have already been mapped and described by Moore et al. (2013) as displacing surface ridges within the Imbricate Thrust Zone.

4.1 NE-trending faults (shallow-deep)

Main structures within the NAP comprise curved NE-trending (azimuth: 40° to 60°) thrusts and back-thrusts dipping toward the NW and SE (Moore et al., 2001) (Figs. 2A–B, 3A–C, 4A and 4C). Thrust faults are clearly associated with the formation of SE-verging anticlines with bathymetric expression on the sea floor (Figs. 1, 2A–B, 3 and 4). Kinematic indicators in these thrusts reveal a secondary right-lateral component in the form of: (1) an increase in the number of back-thrusts in the larger anticlines toward NE, a character denoting accumulation of strain in this same direction; (2) possible horse-tail splay terminations of thrusts occurring at their NE tips (Fig. 3A–B); and (3) slight vergence of hanging-wall anticlines toward the NE (Fig. 4C). Note that kinematic indicators are not observed in all thrusts.

316 Most of the shallow and shorter NE-trending thrusts are clearly primary structures, as they are intersected by
317 or offset other faults with different trends (Fig. 4A). Yet, the deep and large-scale thrusts do not seem to be
318 affected by the same structures (Fig. 4A and C). Whether the deep thrusts are older structures displaced by
319 younger faults with different trends, or these younger faults propagate from deeper thrusts, is a point under
320 discussion as we cannot ascertain clear cross-cutting relationships among all interpreted structures. Either
321 way, the observed geometries suggest that faults are diachronous; the larger, deeper thrusts moved before and
322 after the time of formation of the remaining faults with different trends.

323 The deep thrust faults root in (or start from) the décollement, usually at a depth between 6.5 and 8 km, only
324 intersecting it in the frontal part of the NAP (Fig. 2A–B). In addition, the deep thrusts usually show synthetic
325 (but shallow) thrust faults and antithetic back-thrusts (Fig. 2A–B, 4A and 4C).

326

327 **4.2 WNW- to E-W-trending faults (shallow-deep)**

328 One of the most striking features in the NAP is the steeply dipping WNW-trending F1 fault (azimuth: 110° -
329 115°), a structure ~8 km long and ~3km high, at places intersecting the basal décollement and subduction
330 channel (Fig. 1, 3A–C and 4B–C). The geometry and dip direction of F1 are not constant, suggesting linkage
331 of WNW-trending faults during its formation. Fault F1 displaces the majority of thrust anticlines imaged on
332 seismic data and exhibits a right-lateral strike-slip movement in map view (Fig. 1 and 3A–C). In contrast,
333 vertical seismic profiles reveal normal throws for this same fault (Figs. 4B–C). Its NW tip shows multiple
334 faults with similar trends and slip directions (Fig. 3A–C and 4B). It is not possible to define if these minor
335 faults are branching out of a deeper fault, or if they reflect a highly deformed zone near the sea floor as
336 revealed by the presence of several minor faults (Fig. 4B). Nevertheless, the SE tip of F1 splays out in
337 several branching faults that join or stop against other thrusts (Fig. 3A–C). Similar fault geometries to F1

have been described as negative flower structures in which the horizontal component is dominant (Harding, 1985).

The F1 fault separates two distinct structural domains: (1) a domain to the N where left-lateral slip predominates, and (2) a domain to the S where right-lateral motion is significant (Fig. 3C). At a smaller scale, there are structures with similar kinematics to F1, trending WNW-ESE to E-W (azimuth: 85°–115°), with variable lengths (Fig. 3A–C). These structures comprise a range of pure strike-slip to oblique-slip faults. Their normal slip component (Figs. 3 and 4) can result from normal (dip-slip) movement or comprise an apparent displacement associated with strike-slip motion. The variable throw values recorded, usually increasing toward the surface, together with contrasts between total offset and its bathymetric expression (Fig. 3D), indicate that the observed normal slip can be an apparent slip from right-lateral faults intersecting an inherited fold-and-thrust structure dipping to the NW (Fig. 4C). Furthermore, trend-parallel horizontal offsets are much larger than fault throws, up to a factor of 2 to 3 (Fig. 3C–D). It is important to highlight that not all WNW to E-W structures show lateral movement, suggesting that strike-slip motion is recent or periodically alternates in response to the reactivation of deep structures in the NAP.

Despite F1 being a deep structure that reaches, and seemingly intersects, the décollement, not all WNW to E-W faults propagate beyond a depth of 1 km below the sea floor. However, when compared with other strike-slip faults, WNW to E-W faults are much deeper. Similar fault patterns have been found on other convergent margins, but at larger scales of observation (Lewis et al., 1988; Platt et al., 1988).

4.3 NNW- to N-trending faults (predominantly shallow)

In the outer wedge of the NAP there are several NNW- and N- trending structures (azimuth: 345°–10°) dipping toward the W or sub- vertical, rarely reaching the sea floor (Fig. 3A–C and 4). These faults normally

360 exhibit a left-lateral strike-slip motion, and a variable normal throw (Fig. 3C). Faults trending N to NNW
361 show variable lengths but usually occur in thrust anticlines, rarely extending into their adjacent synclines.
362 Their vertical extension is variable, from a few meters to hundreds of meters, seldom affecting the sea floor.
363 In some cases, similar structures are observed on both the hanging-wall and footwall of major thrust faults,
364 intersecting some of the deeper thrusts in the NAP (Fig. 4A and C).

365

366 **4.4 Normal faults**

367 Minor normal faults on the scale of tens of meters have been observed and are normally confined to the
368 uppermost part of the sediment cover, as previously described by Strasser et al. (2011) and Van Tuyl et al.
369 (2015). These minor faults tend to follow the trends of strike-slip faults, but seldom those of thrust faults
370 (Fig. 5). The normal faults following the trend of strike-slip faults have been classified as normal as they
371 show minor throws without any evidence for horizontal movement. However, they can comprise oblique-slip
372 faults in which their horizontal displacement is below the horizontal seismic resolution of the 3D PSDM
373 volume.

374

375 **4.5 Deep structures**

376 Some of the structures previously identified by Tsuji et al. (2013) as affecting the décollement or units below
377 were also mapped in this work. These deep structures normally show a larger complexity in their geometry
378 and kinematics (Figs. 2B, 6 and 7). According to Tsuji et al. (2013), some of the deep faults imaged on
379 seismic data are inherited structures from Philippine Sea Plate's oceanic crust. These inherited structures do
380 not only control the thickness of the accretionary prism, but also its structural framework. These structures
381 include active intra- oceanic thrusts (Fig. 2B) and some strike-slip faults resulting from lateral movement at

382 the edges of the thicker parts of the NAP. In the outer wedge of the NAP, these intra-oceanic thrusts will
383 control the location of main thrust faults within the Imbricate Thrust Zone. How- ever, in this work we
384 identified several deep-rooted faults with similar directions to the previously described strike-slip faults.

385 Despite their larger structural complexity, deep structures show similar trends to features observed in the
386 NAP, especially when referring to strike-slip fault families (Fig. 6). It is equally important to highlight that
387 these deep structures reach depths larger than 6 km below the sea floor, rooting at and displacing the
388 décollement and underlying units. Some of these structures show relative displacements that do not laterally
389 or vertically agree with a pure extensional or compressional regime of deformation (Fig. 6). Thus, only a
390 strike-slip or a combined regime of deformation can justify such a displacement pattern. This combined
391 regime often generates distributed deformation zones in which strike-slip motions may not be the same as the
392 regional strike-slip movement (McKenzie and Jackson, 1986). In addition, branching and splaying of deep
393 structures are observed and increase upward, resulting in a continuous decrease in the displacement of these
394 splays/branches and, consequently, in a shallower chaotic zone of fracturing that rarely offsets the sea floor
395 (Fig. 6). The fact that these branched faults (and fault F1) reach the sea floor, suggests they may be active or
396 were recently active.

397 As previously discussed, fault F1 is a deep fault that roots in the décollement or in deeper strata. However,
398 the near-seafloor extension of this fault seems to vary along strike (compare Fig. 4C and Fig. 6). In Fig. 4C,
399 which is located a few kilometers NW from Fig. 6, we observe a sharp fault F1 cutting through the outer
400 wedge of the NAP, reaching the sea floor without any major branching or splaying (see also Fig. 6). This
401 geometry can be related to differential movement of different sets of the minor faults that compose fault F1,
402 or to the geometrical interaction between this and other faults, such as fault F2 (Fig. 3).

403 Significant displacement is observed in Unit C in other areas of the outer wedge of NAP, in addition to the
404 area shown in Fig. 6, and con- firms a positive correlation between deformation in the décollement and

underlying units, and deformation in Unit A (Fig. 7). Thus when the oceanic crust, Unit C and, consequently, the décollement are folded and fractured, Unit A usually presents a much greater deformation and structural complexity (see Tsuji et al., 2013).

In Fig. 7B two faults follow the same strike (and are in the same position) of strike-slip fault F1, displacing Unit B and branching upward into a chaotic deformation zone within the entire overlying Unit A. These deep structures have a throw of 500–1000 m, which is significantly larger than the throws of any other thrust in the outer wedge of the NAP, and larger than the horizontal displacement of F1 (ca. 600 m). These thrust faults were previously interpreted as a single major intra-oceanic thrust (Tsuji et al., 2009; Tsuji et al., 2013). Once more, it is possible to observe an upward decrease in their throws, probably occurring in association with splaying/branching towards shallower strata. The observed geometry suggests a variation from a deep regime where dip-slip displacement is larger than horizontal dis- placement, to a shallow regime where dip-slip displacement is smaller than horizontal displacement.

5. DISCUSSION

5.1 Significance of strike-slip faulting in the outer wedge of NAP

Despite clear evidence for primary compressional deformation across the NAP (Moore et al., 2007; Kimura et al., 2007; Kimura et al., 2011), the analysis in this paper reveals that strain in this region is also accommodated by secondary strike-slip deformation. This observation has a significant impact in the structural framework of the NAP and the way(s) stress release and accumulation occur in the region. Therefore, the outer wedge of the NAP is being affected by two main families of strike-slip faults; WNW-trending to E-W right-lateral faults, and NNW- to N-trending left-lateral faults. Their spatial distribution is controlled by F1, which divides two different structural domains. The fact that: (1) the horizontal

127 displacement (120–600 m) is two or three times larger than dip-slip displacement (< 40 m), (2) fault throws
128 are variable in both its magnitude and nature of movement, and (3) normal slip in faults does not have the
129 same expression on the sea floor, lead us to consider these structures to be strike-slip faults (Fig. 3). We
130 interpret that most of the normal slip observed is an apparent slip developed in a fold-and-thrust sequence
131 dipping to the NW, itself affected by strike-slip faulting with significant lateral motion (Fig. 4). Lateral
132 movement is particularly noted on structural maps, where the WNW- to E-W trending and the NNW- to N-
133 trending strike-slip faults are conjugate (Fig. 3).

134 Fig. 4B exhibits a likely negative flower structure with an associated normal-slip component suggesting that,
135 within a dominant transpressional regime, there could be local zones in which transtension is favored in a
136 distributed deformation pattern (McKenzie and Jackson, 1986). This 'flower structure' can also result from
137 the combined effect of strike-slip and thrust movements as: (1) the structural domain to the N of F1 exhibits
138 larger horizontal shortening and tilting than the S domain (Fig. 8), and (2) the curved shape of the NW tip of
139 F1 exhibits a larger throw and horizontal slip as its angle approaches a direction perpendicular to the trench.
140 This is the first mention of flower structures in the Imbricate Thrust and Frontal Thrust Zones of the NAP, al-
141 though other flower structures have been identified in parts of the Nankai Trough and associated with a
142 lateral component of motion (Le Pichon et al., 1996; Takahashi et al., 2002).

143 There are several structures that follow the same orientation as these conjugate strike-slip faults, but without
144 revealing lateral slip. These structures are relatively shallow and exhibit small normal slips to no dip-slip
145 displacement (Figs. 4C and 5). Also, they do not have any bathymetric expression. These latter structures can
146 result from one of two scenarios: (1) blocks bordered by well-developed strike-slip faults experienced some
147 torsion/rotation that is accommodated by extension, (2) accommodation of lateral movement in blocks
148 bordered by strike- slip faults is no longer possible, or is significantly hindered, with new strike-slip or
149 oblique-slip faults being formed as a result.

The observation that deep structures affecting the décollement and underlying units follow the direction of shallow structures (Figs. 1, 6 and 7), highlights the fact that the uppermost strata in the outer wedge of the NAP (Unit A) is influenced by deeper faults. Some of these latter faults have been identified as inherited structures from the subducted Philippine Sea Plate (Tsuji et al., 2013). The fact that some strike-slip faults branch upward, affecting the sea floor, indicates that the outer wedge is slipping during inter-seismic periods and strain is accommodated as transpressional deformation. Fig. 1 shows that some of the thrusts offsetting Unit C and the décollement may not be related to an inherited structure from the Philippines Sea Plate. Considering that some of these thrust faults reach the sea floor, affecting the local bathymetry, they may not be entirely associated with tectonic activity along the MSFZ but, instead, with faulting in Unit C and overlying décollement.

The interpreted seismic volume points to a compressional accretionary prism where synthetic and antithetic thrusts and strike-slip faults are the major structures responsible for deformation in the outer wedge of the NAP, and provides scant evidence for extensional de- formation. However, a dominant strike-slip or compressional de- formation can be responsible for the formation of near-seafloor extensional structures due to gravitational collapse or through the accommodation of deformation at shallower levels of the NAP (Fig. 5), as recorded in other compressional settings (Shelton, 1984; Burchfiel and Royden, 1985). Therefore, we corroborate the presence of a variable ECD within the NAP that is strictly associated with the thickness of the sediment cover (Van Tuyl et al., 2015). In the NAP, the dominant deformation style is not extensional and the shallower extensional regime is a consequence of a dominant transpressional regime.

5.2 Estimates of maximum horizontal stress

Thrust and strike-slip faults identified on seismic attribute maps had their strikes measured for statistical purposes, and to identify the range of strikes for each fault family (Fig. 3). The measured range of strikes was

173 simplified to a mean azimuth so we could apply a dihedral angle method (Hancock, 1985) to interpret the
174 maximum horizontal stress or paleostress responsible for the structures described in this paper. We recognize
175 this latter method as simplistic, but still comprising a valid approach for determining the principal stresses at
176 the time of failure. According to Hancock (1985), an extension fracture is initiated perpendicularly to σ3 in
177 the principal stress plane containing σ1 and σ2, and conjugate hybrid or shear fractures enclose an acute
178 bisector parallel to σ1 (Hancock, 1985). When applying this method, we used two-dimensional strike data
179 from attribute seismic maps and, as a result, we only estimate the maximum horizontal stress.

180 The mean azimuth of the NE-trending thrusts and back-thrusts is 50°. If we were to consider a pure
181 compressional regime for the formation of the NAP, we would infer a maximum horizontal stress trending
182 perpendicularly to this fault family, i.e. 130°. However, as previously discussed in this work, the NAP
183 accretionary prism is characterized by a dominant strike-slip fault regime arranged in a conjugate geometry,
184 where one of the families (NNW- and N-trending) has a mean azimuth of ~357.5° and the other (WNW-ESE
185 to E-W trending) has as a mean azimuth of ~100°. The calculated bihedral/bisector (θ) angle of this conjugate
186 system is ~38.75°, a value that is larger than the 30° generally defined by the Anderson's Theory (Anderson,
187 1905). How- ever, Anderson (1905) and Hancock (1985) postulate that in natural conditions θ should be <
188 40°–45°, depending on the confining pressure

189 and resistance to failure of deformed strata, as the value θ = 30° was calculated in laboratorial conditions for
190 isotropic and mainly non-natural material. The existence of an abnormal pore-fluid pressure within the NAP
191 (Tsuji et al., 2008; Kodaira et al., 2004) justifies the larger dihedral angle calculated here, as it normally
192 increases proportionally to the confining compressive pressure (Ramsey and Chester, 2004). Ismat (2015)
193 defends that the dihedral angle can also increase within the hinge regions of folds, which is one of the main
194 structural features of the NAP.

The bihedral angle of ~38.75° calculated in this work places the maximum horizontal stress at an average azimuth of 138.75°. This is not far from the mean azimuth of 130° inferred from thrust and back- thrust faults in the study area, thus representing a difference of 8.75°. It also represents a difference of < 20° from the general convergence vector of azimuth 120°–125° defined by DeMets et al. (2010). However, Tsuji et al. (2014) state that the convergence vector can deviate up to 30° from the orthogonal direction to the trench, meaning that the calculated mean azimuth for the maximum horizontal stress can also be influenced by this angular relationship.

The minor difference between the azimuths inferred from NE- trending thrusts, and the strike-slip conjugate system, can be related to: (1) a minor rotation of the stress field due to either progressive de- formation or alternating seismic and inter-seismic periods, as suggested by Wang and Hu (2006), or (2) related to the existence of a pre-existing NE-trending structures in the anticlines and (deep) structures inherited from the subducting Philippines Sea Plate (Tsuji et al., 2013). In this latter case, deep structures may have controlled the strain accommodation and stress response within the NAP, particularly when strike- slip becomes the favored regime of deformation.

It was not possible to calculate the exact azimuth of the convergence vector in the study area, but our analysis still provides a mean azimuth for the maximum horizontal stress. Despite the high probability of a σ_{Hmax} parallel to the convergence vector between the Amur and the Philippine Sea Plates, we must assume they do not match. We must also assume that any mismatches between the calculated azimuth for maximum horizontal stress, and the azimuth for the convergence vector, may be due to structural complexity in the NAP or angular errors associated with our geometric analysis - which was purely based on the interpretation of 3D seismic data. Structural complexity is related to the diffuse accommodation of strain in the outer wedge of the NAP, caused by the presence of inherited deep structures (Tsuji et al., 2013) that control the deformation in the upper part of the outer wedge, even with a main convergence vector of azimuth 120°-125°.

519 We recognize that our estimations for the stress state in the outer wedge of the NAP represent a past average
520 stress state. However, the fact that some of the strike-slip faults offset the sea floor, and that strike-slip and
521 thrust faults mutually intersect and offset each other, suggests that this stress state may still be active. Such a
522 postulate implies that the outer wedge is not experiencing a period of coseismic relaxation and, instead, is
523 being compressed by possible aseismic slip of subduction faults (Wang and Hu, 2006).

524

525 **5.3 Deformation styles in the outer wedge of the NAP and comparison with other accretionary prisms**

526 In the Kumano Basin, Moore et al. (2013) identified four populations of normal faults in strata overlying the
527 NAP. They share similar trends to faults interpreted in this paper (Figs. 9A–B). Phase 1 normal faults
528 correspond to our NE-trending thrust and back-thrust faults, whereas phase 2 and phase 3 normal fault
529 populations respectively match the orientation of NNW- to N-trending left-lateral strike-slip faults and
530 WNW-trending to E-W right-lateral strike-slip faults. This character suggests that normal faults generated in
531 the sediment cover of the NAP, and in Kumano Basin sediment, can be the near-surface expression of
532 gravitational collapse or local adjustments from structures active at deep levels, imposing anisotropic
533 conditions in both the inner and outer wedges of the NAP. Similar syn-sedimentary normal faults have been
534 described for the Makran accretionary prism as responding to prism overthickening caused by underplating
535 (Platt et al., 1988).

536 According to Boston et al. (2016), the inner wedge of the NAP inherited a pre-existing structural framework
537 that is chiefly composed of thrusts similar to those interpreted in the outer wedge. Compression remains the
538 main deformation style operating in the NAP. The structural data collected by Boston et al. (2016) in the
539 inner wedge also agree with the trends of structures and fault families in this work; the majority of the
540 structural data in Boston et al. (2016) correlate with our synthetic thrust faults. The few deep structures

541 identified by Boston et al. (2016) are geometrically related to our strike-slip families (Fig. 9A and C).
542 However, no reference to strike-slip is made in their work.

543 Taking into consideration Moore et al. (2013) and Boston et al. (2016) interpretations, structures within the
544 inner wedge and the Kumano Basin are geometrically similar to structures identified and mapped in this
545 work, and variations in strikes and faulting regimes can be entirely related to strain partitioning from the
546 Frontal Thrust Zone to the inner wedge or related to the MSFZ. This interpretation suggests that structures
547 across the NAP somewhat reflect the same tectonic setting, but result in different structural expressions
548 depending on the local geological and physical conditions. In the outer wedge, there is no evidence for a
549 dominant extensional deformational style, especially when considering that all normal faults are small and
550 follow the same trend of deeper strike-slip (and thrust) faults. Instead, evidence points toward the co-
551 existence of both compressional and strike-slip styles of deformation.

552 Cross-cutting relationships between strike-slip faults and thrusts are not always easy to observe due to the
553 NAP's structural complexity and poorer seismic resolution at depth. However, structural data in this work
554 suggests a primary fold-and-thrust framework that is later intersected by relatively recent thrust and strike-
555 slip structures. The chronology between these latter strike-slip and thrust faults is not conclusive as they seem
556 to have been reactivated simultaneously: 1) as a con- sequence of a transpressional regime, where both
557 thrusting and strike- slip faulting coexist, or 2) due to alternations between co-seismic and inter-seismic
558 periods favouring the generation of thrusts and strike-slip structures in discrete tectonic pulses.

559 We favor the first hypothesis above due to the fact that a transpressional regime, in which both thrusting and
560 strike-slip can develop, corroborates the information discussed in Section 5.2. Furthermore, the chronological
561 order proposed by Moore et al. (2013) for the normal fault populations in the Kumano Basin matches the
562 postulate of an initial fold-and-thrust regime followed by a transpressional regime where thrust and strike-
563 slip faulting coexist, similarly to what is observed in the Shumagin region of the Aleutian Trench (Lewis et

564 al., 1988). The present-day tectonic setting in the NAP is, in fact, very similar to those of the Aleutian Trench
565 and Makran accretionary prism, where Lewis et al. (1988) and Platt et al. (1988) proposed three evolution
566 stages: (1) folding along an axis perpendicular to the plate-convergence direction in the region, (2) thrust
567 faulting in the direction of plate convergence, and (3) oblique strike-slip faulting along conjugate right-lateral
568 and left-lateral faults. These conjugate strike-slip faults clearly post-date the initial fold-and-thrust geometry
569 in both the Aleutian Trench and off- shore Makran, but evolved simultaneously with the major thrusts in the
570 later stages of tectonic shortening. This suggests some overlap between the stages 2 and 3 previously
571 described.

572 Some of the strike-slip faults in the study area (mainly fault F1) are associated with deeper inherited
573 structures affecting the décollement (Tsuji et al., 2013). Most of the left-lateral NNW- to N-trending strike-
574 slip faults are confined within the thrust anticlines and can be associated with a flat-and-ramp setting, where
575 the lateral component of the oblique displacement of thrusts (flat) is transferred as left-lateral dis- placement
576 in strike-slip faults (ramp) (Platt et al., 1988; Cunningham, 2005).

577 The presence of negative flower structures, when considered together with the branching of faults on seismic
578 and attribute data (Fig. 4B and 8), suggests the occurrence of a transtensional regime (Sanderson and
579 Marchini, 1984). As faults are very localized, and no major normal faults are observed in the study area, we
580 interpret transtension as a consequence of the accommodation and partitioning of all transpressional
581 deformation in the outer wedge of the NAP. The fact that there are no major normal faults within the outer
582 wedge of the NAP, and that strike-slip is more common, indicates that strike-slip faulting is still
583 accommodating the shortening of the outer wedge of the NAP, and that the maximum horizontal stress is, in
584 fact, the direction of maximum compression ($\sigma 1$) for the study area (Fig. 9A).

585

586 **6. CONCLUSIONS**

This work shows that the outer wedge of the NAP is a compressional region broadly affected by folding-and-thrusting and a secondary, but still important, strike-slip faulting regime. In particular, the study area is affected by three major types of structures: (1) a regional fold-and- thrust setting of synthetic thrusts, antithetic thrusts and corresponding anticlines; (2) localized conjugate families of strike-slip faults comprising left-lateral NNW- to N-trending faults and right-lateral WNW- to E-W trending faults. Within this latter family there is a major regional right-lateral strike-slip fault (F1) that separates two different structural domains. This strike-slip fault is associated with pre-existing structures affecting the décollement and the upper part of the outer wedge.

Maximum horizontal stress inferred from structures interpreted on seismic data is geometrically close to the convergence vector between the Eurasian and Philippine Sea Plates. Despite being clearly associated with past average stresses, maximum horizontal stress in the outer wedge may still represent the main direction of shortening in the NAP which is, at present, accommodated by strike-slip faults. In this rapidly evolving accretionary system, convergence was initially responsible for widespread compression in the NAP and formation of a fold-and-thrust setting, which progressed into a transpressional regime with thrust and strike-slip faulting occurring simultaneously, or in alternation. There is no evidence for a dominant extensional regime, or a transition from a shallow extensional regime to a deeper compressional or strike-slip regime. Extensional structures and stress decoupling are only visible in regions with significant sediment cover, thus comprising the superficial expression of deeper transpressional tectonics or localized areas of larger structural complexity. The recognition of a transpressional regime operating in the outer wedge of the NAP at present has a significant impact in the stress distribution and consequent accommodation of strain offshore Nankai.

ACKNOWLEDGMENTS

510 This research used seismic data from the Kumano Transect collected by PGS and processed by CGG and
511 IFREE/JAMSTEC. Schlumberger is acknowledged for providing Petrel® software and licenses to the 3D
512 Seismic Lab. We thank the reviewers and editor for their constructive comments, which greatly improved an
513 early version of this manuscript.

514

515 **REFERENCES CITED**

516 Alves, T.M., et al., 2013. Erosional features as indicators of thrust fault activity (Nankai Trough, Japan).
517 Mar. Geol. 356, 5–18. http://dx.doi.org/10.1016/j.margeo.2013.07. 011.

518 Anderson, E.M., 1905. The dynamics of faulting. Transactions of the Edinburgh Geological Society 8 (3),
519 387–402. http://dx.doi.org/10.1144/transed.8.3.387.

520 Bangs, N.L.B., Moore, G.F., Gulick, S.P.S., Pangborn, E.M., Tobin, H.J., Kuramoto, S., Taira, A., 2009.
521 Broad, weak regions of the Nankai Megathrust and implications for shallow coseismic slip. Earth Planet.
522 Sci. Lett. 284, 44–49. http://dx.doi.org/10. 1016/j.epsl.2009.04.026.

523 Boston, B., Moore, G.F., Jurado, M.J., Sone, H., 2016. Deformation of the Nankai Trough inner accretionary
524 prism: the role of inherited structures. Geochemistry Geophysics Geosystem 17, 485–500.
525 http://dx.doi.org/10.1002/2015GC006185.

526 Burchfiel, B.C., Royden, L.H., 1985. North-south extension within the convergent Himalayan region.
527 Geology 13 (10), 679–682. http://dx.doi.org/10.1130/0091- 7613(1985)13<679:NEWTCH>2.0.CO;2.

528 Byrne, D.E., Wang, W.H., Davis, D.M., 1993. Mechanical role of backstops in the growth of forearcs.
529 Tectonics 12 (1), 123–144. http://dx.doi.org/10.1029/92TC00618. Byrne, T.B., Lin, W., Tsutsumi, A.,
530 Yamamoto, Y., Lewis, J.C., Kanagawa, K., Kitamura, Y.,

531 Yamaguchi, A., Kimura, G., 2009. Anelastic strain recovery reveals extension across SW Japan subduction
532 zone. Geophys. Res. Lett. 36 (23). http://dx.doi.org/10.1029/ 2009GL040749.

533 Chang, C., Song, I., 2016. Present-day stress states underneath the Kumano basin to 2 km below seafloor
534 based on borehole wall failures at IODP site C0002, Nankai accre- tionary wedge. Geochem. Geophys.
535 Geosyst. 17. http://dx.doi.org/10.1002/ 2016GC006562.

536 Chopra, S., Marfurt, K.J., 2005. Seismic attributes—a historical perspective. Geophysics 70 (5), 3SO–28SO.
537 http://dx.doi.org/10.1190/1.2098670.

538 Chopra, S., Marfurt, K., 2007a. Curvature attribute applications to 3D surface seismic data. Lead. Edge 26
539 (4), 404–414. http://dx.doi.org/10.1190/1.2723201.

540 Chopra, S., Marfurt, K.J., 2007b. Volumetric curvature attributes for fault/fracture characterization. First
541 Break 25 (7), 35–46. http://dx.doi.org/10.3997/1365–2397. 2007019.

542 Cunningham, D., 2005. Active intracontinental transpressional mountain building in the Mongolian Altai:
543 defining a new class of orogeny. Earth Planet. Sci. Lett. 240 (2), 436–444.
544 http://dx.doi.org/10.1016/j.epsl.2005.09.013.

545 Dahlen, F.A., Suppe, J., Davis, D., 1984. Mechanics of fold-and-thrust belts and accre- tionary wedges:
546 cohesive Coulomb theory. J. Geophys. Res. Solid Earth 89 (B12), 10087–10101.
547 http://dx.doi.org/10.1029/JB089iB12p10087.

548 Davis, D., Suppe, J., Dahlen, F.A., 1983. Mechanics of fold-and-thrust belts and accre- tionary wedges. J.
549 Geophys. Res. Solid Earth 88 (B2), 1153–1172. http://dx.doi.org/ 10.1029/JB088iB02p01153.

550 DeMets, C., Gordon, R.G., Argus, D.F., 2010. Geologically current plate motions. Geophys. J. Int. 181 (1),
551 1–80. http://dx.doi.org/10.1111/j.1365-246X.2009.04491.x.

552 Expedition 315 Scientists, 2009. Expedition 315 Site C0001: Proceedings of the Integrated Ocean Drilling
553 Program. vol. 314/315/316http://dx.doi.org/10.2204/iodp.proc. 314315316.123.2009.

554 Expedition 316 Scientists, 2009. Expedition 316 Site C0006. In: Kinoshita, M., Tobin, H., Ashi, J., Kimura,
555 G., Lallemant, S., Screaton, E.J., Curewitz, D., Masago, H., Moe, K.T. (Eds.), The Expedition
556 314/315/316 Scientists, Proc. IODP, 314/315/316, http://dx.
557 doi.org/10.2204/iodp.proc.314315316.134.2009.

558 Expedition 333 Scientists, 2012. Site C0018. In: Henry, P., Kanamatsu, T., Moe, K. (Eds.), The Expedition
559 333 Scientists, Proc. IODP, 333. Integrated Ocean Drilling Program Management International, Inc.,
560 Tokyo. http://dx.doi.org/10.2204/iodp.proc.333. 103.2012.

561 Gulick, S.P.S., Bangs, N.L.B., Shipley, T.H., Nakamura, Y., Moore, G., Kuramoto, S., 2004. Three-
562 dimensional architecture of the Nankai accretionary prism's imbricate thrust zone off Cape Muroto,
563 Japan: prism reconstruction via en echelon thrust propagation. J. Geophys. Res. Solid Earth 109 (B2),
564 1978–2012. http://dx.doi.org/10.1029/ 2003JB002654.

565 Hancock, P.L., 1985. Brittle microtectonics: principles and practice. J. Struct. Geol. 7 (3), 437–457.
566 http://dx.doi.org/10.1016/0191-8141(85)90048-3.

567 Harding, T.P., 1985. Seismic characteristics and identification of negative flower struc- tures, positive flower
568 structures, and positive structural inversion. AAPG Bull. 69 (4), 582–600.

569 Huffman, K.A., Saffer, D.M., 2016. In situ stress magnitudes at the toe of the Nankai trough accretionary
570 prism, offshore Shikoku Island, Japan. J. Geophys. Res. Solid Earth 121, 1202–1217.
571 http://dx.doi.org/10.1002/2015JB012415.

572 Ismat, Z., 2015. What can the dihedral angle of conjugate-faults tell us? J. Struct. Geol. 73, 97–113.
573 http://dx.doi.org/10.1016/j.jsg.2015.02.008.

574 Kamei, R., Pratt, R.G., Tsuji, T., 2012. Waveform tomography imaging of a megasplay fault system in the
575 seismogenic Nankai subduction zone. Earth Planet. Sci. Lett. 317, 343–353.
576 http://dx.doi.org/10.1016/j.epsl.2011.10.042.

577 Kimura, G., Kitamura, Y., Hashimoto, Y., Yamaguchi, A., Shibata, T., Ujiie, K., Okamoto, S.Y., 2007.
578 Transition of accretionary wedge structures around the up-dip limit of the seismogenic subduction zone.
579 Earth Planet. Sci. Lett. 255 (3), 471–484. http://dx.doi. org/10.1016/j.epsl.2007.01.005.

580 Kimura, G., Moore, G.F., Strasser, M., Screaton, E., Curewitz, D., Streiff, C., Tobin, H., 2011. Spatial and
581 temporal evolution of the megasplay fault in the Nankai Trough. Geochem. Geophys. Geosyst. 12 (3).
582 http://dx.doi.org/10.1029/2010GC003335.

583 Kodaira, S., Iidaka, T., Kato, A., Park, J.O., Iwasaki, T., Kaneda, Y., 2004. High pore fluid pressure may
584 cause silent slip in the Nankai Trough. Science 304 (5675), 1295–1298.
585 http://dx.doi.org/10.1126/science.1096535.

586 Kodaira, S., Hori, T., Ito, A., Miura, S., Fujie, G., Park, J.-O., Baba, T., Sakaguchi, H., Kaneda, Y., 2006. A
587 cause of rupture segmentation and synchronization in the Nankai trough revealed by seismic imaging
588 and numerical simulation. J. Geophys. Res. 111. http://dx.doi.org/10.1029/2005JB004030.

589 Le Pichon, X., Kobayashi, K., Crew, K.N.S., 1992. Fluid venting activity within the eastern Nankai Trough
590 accretionary wedge: a summary of the 1989 Kaiko-Nankai results. Earth Planet. Sci. Lett. 109 (3), 303–
591 318. http://dx.doi.org/10.1016/0012-821X(92) 90094-C.

592 Le Pichon, X., Wmant, S., Tokuyama, H., Thoue, F., Huchon, P., Henry, P., 1996. Structure and evolution of
593 the backstop in the eastern Nankai trough area (Japan): implications for the soon-to-come Tokai
594 earthquake. Island Arc 5 (4), 440–454. http://dx.doi.org/ 10.1111/j.1440-1738.1996.tb00164.x.

Lewis, S.D., Ladd, J.W., Bruns, T.R., 1988. Structural development of an accretionary prism by thrust and strike-slip faulting: Shumagin region, Aleutian Trench. Geol. Soc. Am. Bull. 100, 767–782.

Lewis, J.C., Byrne, T.B., Kanagawa, K., 2013. Evidence for mechanical decoupling of the upper plate at the Nankai subduction zone: constraints from core-scale faults at NantroSEIZE Sites C0001 and C0002. Geochem. Geophys. Geosyst. 14 (3), 620–633. http://dx.doi.org/10.1029/2012GC004406.

Lin, W., Byrne, T.B., Kinoshita, M., McNeill, L.C., Chang, C., Lewis, J.C., Yamamoto, Y., Saffer, D.M., Casey Moore, J., Wu, H.-Y., Tsuji, T., Yamada, Y., Conin, M., Saito, S., Ito, T., Tobin, H.J., Kimura, G., Kanagawa, K., Ashi, J., Underwood, M.B., Kanamatsu, T., 2015. Distribution of stress state in the Nankai subduction zone, southwest Japan and a comparison with Japan Trench. Tectonophysics 692, 120–130. http://dx.doi. org/10.1016/j.tecto.2015.05.008.

MacKay, M.E., Moore, G.F., Cochrane, G.R., Casey Moore, J., Kulm, LaVerne D., 1992. Landward vergence and oblique structural trends in the Oregon margin accretionary prism: Implications and effect on fluid flow. Earth Planet. Sci. Lett. 109 (3–4), 477–491.

Mai, H.T., Marfurt, K.J., Chávez-Pérez, S., 2009. Coherence and volumetric curvatures and their spatial relationship to faults and folds, an example from Chicontepec basin, Mexico. In: SEG Technical Program Expanded Abstracts. vol. 2009. pp. 1063–1067. http://dx.doi.org/10.1190/1.3255033.

Martin, K.M., Gulick, S.P.S., Bangs, N.L.B., Moore, G.F., Ashi, J., Park, J.-O., Kuramoto, S., Taira, A., 2010. Possible strain partitioning structure between the Kumano fore-arc basin and the slope of the Nankai Trough accretionary prism. Geochem. Geophys. Geosyst. 11http://dx.doi.org/10.1029/2009GC002668. (Q0AD02).

McKenzie, D., Jackson, J., 1986. A block model of distributed deformation by faulting. J. Geol. Soc. 143 (2), 349–353. http://dx.doi.org/10.1144/gsjgs.143.2.0349.

Miyazaki, S.I., Heki, K., 2001. Crustal velocity field of southwest Japan: subduction and arc-arc collision. J. Geophys. Res. Solid Earth 106 (B3), 4305–4326. http://dx.doi. org/10.1029/2000JB900312.

Moore, Gregory F., Taira, A., Klaus, A., Becker, L., Boeckel, B., Cragg, B.A., Dean, A., Fergusson, C.L., Henry, P., Hirano, S., Hisamitsu, T., Hunze, S., Kastner, M., Maltman, A.J., Morgan, J.K., Murakami, Y., Saffer, D.M., Sánchez-Gómez, M., Screaton, E.J., Smith, D.C., Spivack, J.A., Steurer, J., Tobin, H.J., Ujiie, K., Underwood, M.B., Wilson, M., 2001. New insights into deformation and fluid flow processes in the Nankai Trough accretionary prism: results of ocean drilling program leg 190. Geochem. Geophys. Geosyst. 2.

Moore, G.F., Bangs, N.L., Taira, A., Kuramoto, S., Pangborn, E., Tobin, H.J., 2007. Three- dimensional splay fault geometry and implications for tsunami generation. Science 318 (5853), 1128–1131. http://dx.doi.org/10.1126/science.1147195.

Moore, G.F., Park, J.-O., Bangs, N.L., Gulick, S.P., Tobin, H.J., Nakamura, Y., Sato, S., Tsuji, T., Yoro, T., Tanaka, H., Uraki, S., Kido, Y., Sanada, Y., Kuramoto, S., Taira, A., 2009. Structural and seismic stratigraphic framework of the NanTroSEIZE Stage 1 transect. In: Kinoshita, M., Tobin, H., Ashi, J., Kimura, G., Lallemant, S., Screaton, E.J., Curewitz, D., Masago, H., Moe, K.T., the Expedition 314/315/316 Scientists (Eds.), Proc. IODP, 314/315/316. (Integrated Ocean Drilling Program Management International, Inc.), Washington, DC. http://dx.doi.org/10.2204/iodp.proc. 314315316.102.2009.

Moore, G.F., Boston, B.B., Sacks, A.F., Saffer, D.M., 2013. Analysis of normal fault po- pulations in the Kumano Forearc Basin, Nankai Trough, Japan: 1. Multiple orienta- tions and generations of faults from

737 3-D coherency mapping. Geochem. Geophys. Geosyst. 14 (6), 1989–2002.
738 http://dx.doi.org/10.1002/ggge.20119.

739 Moore, G.F., Boston, B.B., Strasser, M., Underwood, M.B., Ratliff, R.A., 2015. Evolution of tectono-
740 sedimentary systems in the Kumano Basin, Nankai trough forearc. Mar. Pet.

741 Geol. 67, 604–616. http://dx.doi.org/10.1016/j.marpetgeo.2015.05.032. Obana, K., Kodaira, S., Kaneda, Y.,
742 2005. Seismicity in the incoming/subducting

743 Philippine Sea plate off the Kii Peninsula, central Nankai trough. J. Geophys. Res.

744 110. http://dx.doi.org/10.1029/2004JB003487.

745 Park, J.O., Tsuru, T., Kaneda, Y., Kono, Y., Kodaira, S., Takahashi, N., Kinoshita, H., 1999.

746 A subducting seamount beneath the Nankai accretionary prism off Shikoku, south- western Japan. Geophys.
747 Res. Lett. 26 (7), 931–934. http://dx.doi.org/10.1029/ 1999GL900134.

748 Park, J.O., Tsuru, T., Kodaira, S., Cummins, P.R., Kaneda, Y., 2002. Splay fault branching along the Nankai
749 subduction zone. Science 297 (5584), 1157–1160. http://dx.doi. org/10.1126/science.1074111.

750 Park, J.-O., Fujie, G., Wijerathne, L., Hori, T., Kodaira, S., Fukao, Y., Moore, G.F., Bangs, N.L., Kuramoto,
751 S., Taira, A., 2010. A low-velocity zone with weak reflectivity along the Nankai subduction zone.
752 Geology 38 (3), 283–286. http://dx.doi.org/10.1130/ G30205.1.

753 Platt, J.P., Leggett, J.K., Alam, S., 1988. Slip vectors and fault mechanics in the Makran accretionary wedge,
754 southwest Pakistan. J. Geophys. Res. Solid Earth 93 (B7), 7955–7973.

755 Ramsey, J.M., Chester, F.M., 2004. Hybrid fracture and the transition from extension fracture to shear
756 fracture. Nature 428 (6978), 63–66. http://dx.doi.org/10.1038/ nature02333.

757 Roberts, A., 2001. Curvature attributes and their application to 3 D interpreted horizons. First Break 19 (2),
758 85–100. http://dx.doi.org/10.1046/j.0263-5046.2001.00142.x.

759 Sanderson, D.J., Marchini, W.R.D., 1984. Transpression. J. Struct. Geol. 6 (5), 449–458.
760 http://dx.doi.org/10.1016/0191-8141(84)90058-0.

761 Shelton, J.W., 1984. Listric normal faults: an illustrated summary. AAPG Bull. 68 (7), 801–815.

762 Strasser, M., Moore, G.F., Kimura, G., Kopf, A.J., Underwood, M.B., Guo, J., Screaton, E.J., 2011.
763 Slumping and mass transport deposition in the Nankai fore arc: evidence from IODP drilling and 3-D
764 reflection seismic data. Geochem. Geophys. Geosyst. 12 (5). http://dx.doi.org/10.1029/2010GC003431.

765 Strasser, M., Dugan, B., Kanagawa, K., Moore, G.F., Toczko, S., Maeda, L., The Expedition 338 Scientists,
766 2014. Site C0018: Proceedings of the Integrated Ocean Drilling Program. vol. 338. pp. 2.
767 http://dx.doi.org/10.2204/iodp.proc.338.105.2014.

768 Takahashi, N., Amano, H., Hirata, K., Kinoshita, H., Lallemant, S., Tokuyama, H., Tamamoto, F., Taira, A.,
769 Suyehiro, K., 2002. Faults configuration around the eastern Nankai trough deduced by multichannel
770 seismic profiling. Mar. Geol. 187 (1), 31–46. http://dx.doi.org/10.1016/S0025-3227(02)00243-8.

771 Tobin, H.J., Kinoshita, M., 2006. NanTroSEIZE: the IODP Nankai Trough seismogenic zone experiment.
772 Sci. Drill. 2 (2), 23–27. http://dx.doi.org/10.2204/iodp.sd.2.06. 2006.

773 Tsuji, T., Tokuyama, H., Costa Pisani, P., Moore, G., 2008. Effective stress and pore pressure in the Nankai
774 accretionary prism off the Muroto Peninsula, southwestern Japan. J. Geophys. Res. Solid Earth 113
775 (B11). http://dx.doi.org/10.1029/ 2007JB005002.

776 Tsuji, T., Park, J.-O., Moore, G., Kodaira, S., Fukao, Y., Kuramoto, S., Bangs, N., 2009. Intraoceanic thrusts
777 in the Nankai Trough off the Kii Peninsula: implications for in- traplate earthquakes. Geophys. Res. Lett.
778 36, L06303. http://dx.doi.org/10.1029/ 2008GL036974.

779 Tsuji, T., Kodaira, S., Ashi, J., Park, J.O., 2013. Widely distributed thrust and strike-slip faults within
780 subducting oceanic crust in the Nankai Trough off the Kii Peninsula, Japan. Tectonophysics 600, 52–62.
781 http://dx.doi.org/10.1016/j.tecto.2013.03.014.

782 Tsuji, T., Ashi, J., Ikeda, Y., 2014. Strike-slip motion of a mega-splay fault system in the Nankai oblique
783 subduction zone. Earth, Planets Space 66 (1), 1–14. http://dx.doi. org/10.1186/1880-5981-66-120.

784 Van Tuyl, J., Alves, T.M., Moore, G.F., 2015. Strain decoupling reveals variable seismo- genic risk in SE
785 Japan (Nankai Trough). Geochem. Geophys. Geosyst. 16 (7), 2025–2037.
786 http://dx.doi.org/10.1002/2015GC005778.

787 Wang, K., Hu, Y., 2006. Accretionary prisms in subduction earthquake cycles: The theory of dynamic
788 Coulomb wedge. J. Geophys. Res. Solid Earth 111 (B6). http://dx.doi. org/10.1029/2005JB004094.

789 Wu, H.Y., Chan, C.H., Kinoshita, M., Saito, S., 2013. Stress field observation and modeling from the
790 NanTroSEIZE scientific drillings in the Nankai Trough system, SW Japan. Tectonophysics 600, 99–107.
791 http://dx.doi.org/10.1016/j.tecto.2013.04.009.

FIGURES

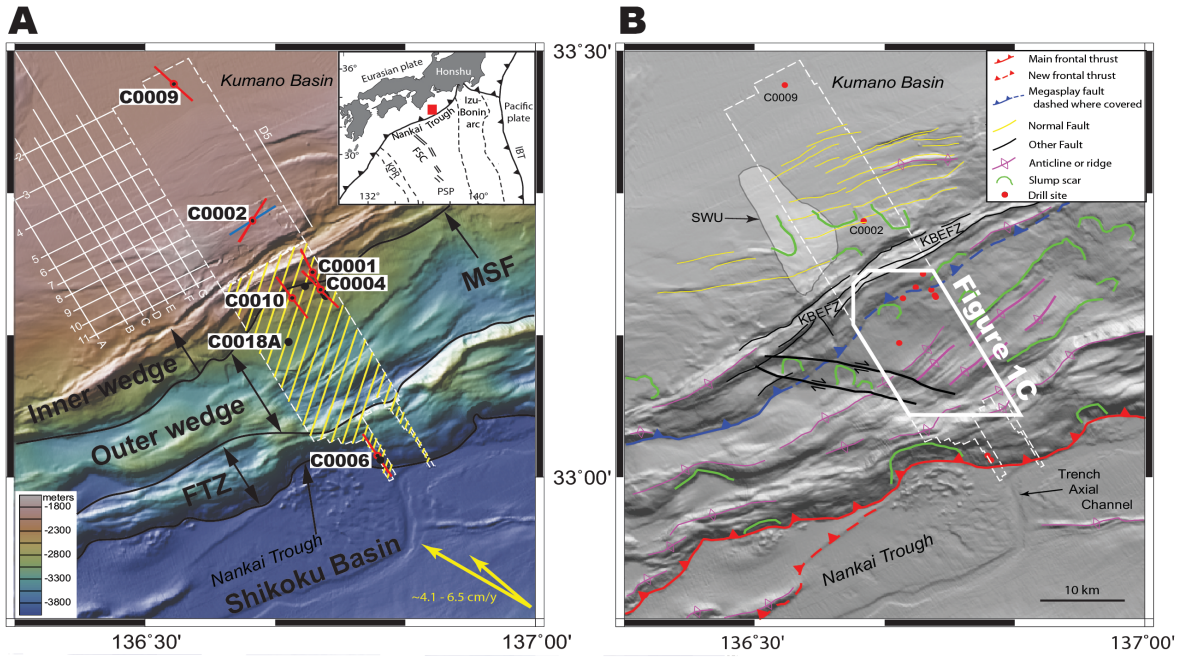
A
B
Kumano Basin
C0009
C0002
C0001
C0004
C0010
C0018A
C0006
MSF
Inner wedge
Outer wedge
FTZ
Nankai Trough
Shikoku Basin
~4.1 - 6.5 cm/y
Eurasian plate
Honshu
Pacific plate
Izu-Bonin arc
Nankai Trough
PSP
meters
-1800
-2300
-2800
-3300
-3800
33°30'
33°00'
136°30'
137°00'
Main frontal thrust
New frontal thrust
Megasplay fault dashed where covered
Normal Fault
Other Fault
Anticline or ridge
Slump scar
Drill site
SWU
KBEFZ
Figure 1C
Trench Axial Channel
10 km

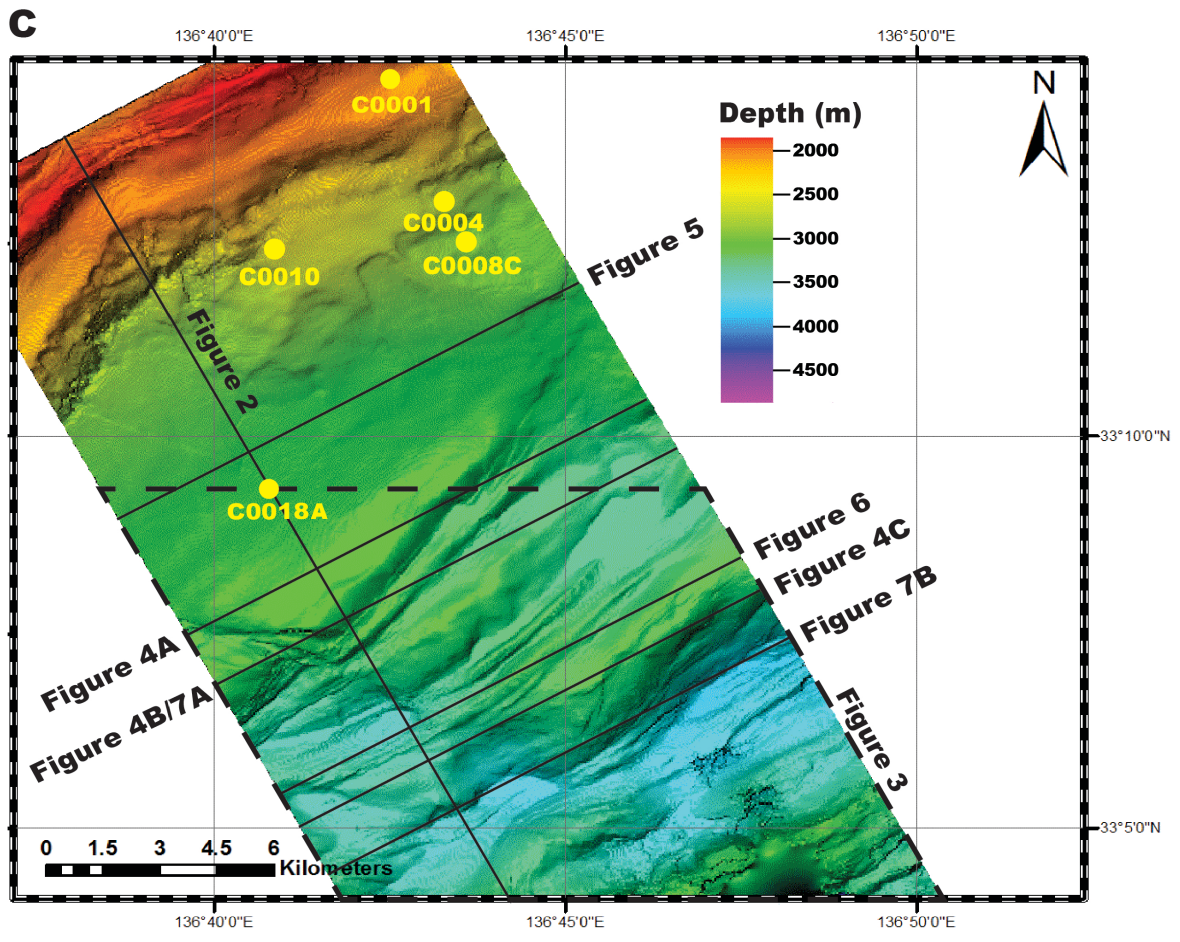
C
136°40'0"E
136°45'0"E
136°50'0"E
33°10'0"N
33°5'0"N
N
Depth (m)
2000
2500
3000
3500
4000
4500
C0001
C0004
C0008C
C0010
C0018A
Figure 2
Figure 3
Figure 4A
Figure 4B/7A
Figure 4C
Figure 5
Figure 6
Figure 7B
0 1.5 3 4.5 6
Kilometers

Fig. 1. A) Relief map of the Kumano Basin region of the Nankai Trough as modified from Moore et al. (2013). The figure shows the location of the 3D seismic volume (white dashed box), maximum horizontal stress directions (red lines and blue line), the location of JAMSTEC 2-D seismic lines (white lines) and convergence vectors between the Philippine Sea Plate and Japan (yellow arrows). Also highlighted in the figure are the study area (yellow lines) and distinct tectonic regions in the NAP as shown in Kimura et al. (2011). The inset shows a regional tectonic map with the present day configuration of the Nankai Trough. MSF - Megasplay Fault; ITZ - Imbricate Thrust Zone; FTZ - Frontal Thrust Zone; KPR- Kyushu-Palau Ridge; FSC - fossil spreading center; PSP - Philippine Sea Plate; IBT - Izu-Bonin Trench. Red box shows the location of the study area in SE Japan. B) Tectonic interpretation from Moore et al. (2013) showing the area interpreted in Fig. 1C. KBEFZ = Kumano Basin Edge Fault Zone; SWU = southwestern uplift. C) Bathymetric map derived from the Kumano 3D seismic volume showing the direction of seismic profiles in this paper and IODP Sites C0001, C0004, C0008C, C0010 and C0018A. The study area comprises the southern limit of the Kumano Transect, up to the MSFZ.

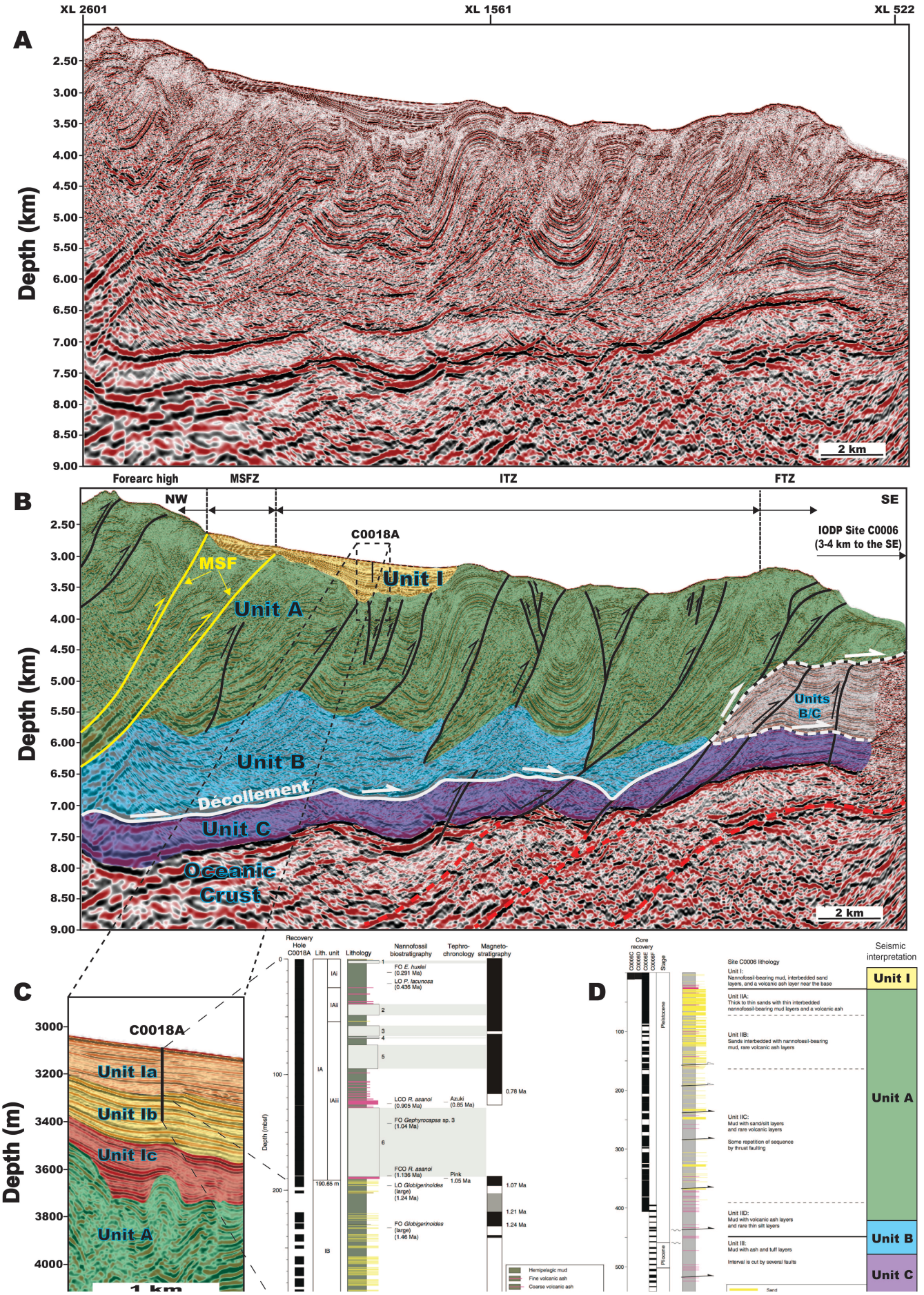
A
XL 2601
XL 1561
XL 522
Depth (km)
2 km
B
Forearc high
MSFZ
ITZ
FTZ
NW
SE
C0018A
IODP Site C0006
(3-4 km to the SE)
MSF
Unit I
Unit A
Units B/C
Unit B
Décollement
Unit C
Oceanic Crust
2 km
C
C0018A
Unit Ia
Unit Ib
Unit Ic
Unit A
Depth (m)
1 km
Recovery
Hole C0018A
Lith. unit
Lithology
Nannofossil biostratigraphy
Tephro-chronology
Magneto-stratigraphy
Depth (mbsf)
190.85 m
FO E. huxlei (0.291 Ma)
LO P. lacunosa (0.435 Ma)
LCO R. asanoi (0.905 Ma)
Azuki (0.85 Ma)
FO Gephyrocapsa sp. 3 (1.04 Ma)
FCO R. asanoi (1.136 Ma)
Pink 1.05 Ma
LO Globigerinoides (large) (1.24 Ma)
FO Globigerinoides (large) (1.46 Ma)
0.78 Ma
1.07 Ma
1.21 Ma
1.24 Ma
Hemipelagic mud
Fine volcanic ash
Coarse volcanic ash
D
Core recovery
Stage
Pleistocene
Pliocene
Site C0006 lithology
Unit I:
Nannofossil-bearing mud, interbedded sand layers, and a volcanic ash layer near the base
Unit IIA:
Thick to thin sands with thin interbedded nannofossil-bearing mud layers and a volcanic ash
Unit IIB:
Sands interbedded with nannofossil-bearing mud, rare volcanic ash layers
Unit IIC:
Mud with sand/silt layers and rare volcanic layers
Some repetition of sequence by thrust faulting
Unit IID:
Mud with volcanic ash layers and rare thin silt layers
Unit III:
Mud with ash and tuff layers
Interval is cut by several faults
Sand
Seismic interpretation
Unit I
Unit A
Unit B
Unit C

Fig. 2. A & B) Depth-migrated seismic profile (Inline 2315) across thrust-and-fold structures in the NAP. The figures also show interpreted (colored and shaded) tectono-stratigraphic units and the location of IODP Site C0018A. Unit I (yellow) represents relatively undeformed slope sediment (Expedition 315 Scientists, 2009; Kimura et al., 2011; Alves et al., 2013; Strasser et al., 2014), whereas Units A (green), B (blue), C (purple) and oceanic crust (colorless) are interpreted based on Park et al. (2010). IODP Site C0006 is 3–4 km distant from the SE end of the seismic profile, meaning that the interpreted seismic units show lateral continuity with the tectono-stratigraphic units shown in Fig. 2D for IODP Site C0006, further southeast. The area labeled as seismic units B/C is open to interpretation as the seismic resolution significantly decreases further SE. (black lines – major thrust and back-thrust faults; arrows – vergence of anticlines and thrusts; white line – décollement fault; dashed white lines – possible décollement paths; dashed red lines – possible faults within the subducted oceanic crust; yellow lines – splays of the MSFZ; MSFZ – Megasplay Fault Zone; ITZ – Imbricate Thrust Zone; FTZ – Frontal Thrust Zone). C) Close-up of IODP well C0018A highlighting the subdivision of Unit I in Units Ia, Ib and Ic based on Strasser et al. (2014). D) Well log from IODP Site C0006 (Expedition 316 Scientists, 2009) tied to the seismic units interpreted in this work. According to Expedition 316 Scientists (2009), Unit III is consistent with deposition in the Shikoku Basin.

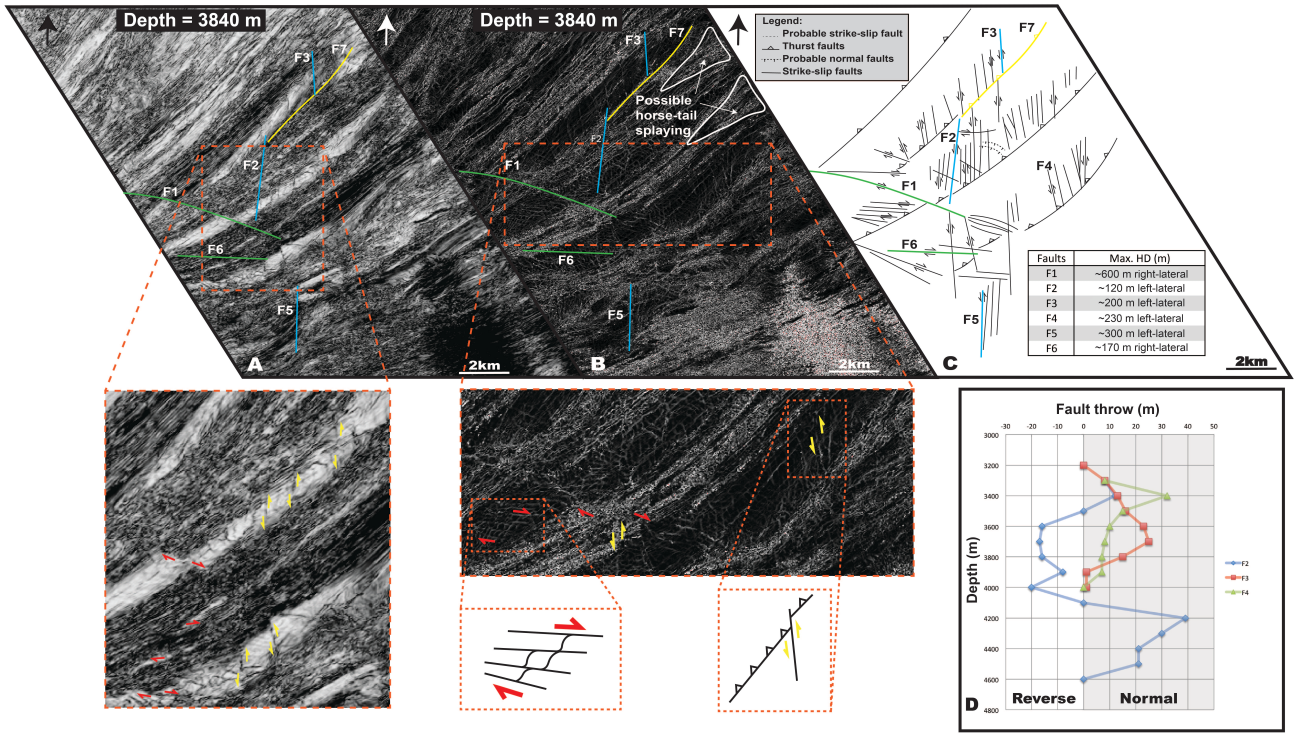

Fig. 3. A & B) Coherence and maximum curvature maps (at a depth of 3840 m) with corresponding zoomed insets showing main structural lineaments and interpreted faults. Red half-arrows – relative right-lateral movement; yellow half-arrows – relative left-lateral movement C) Schematic interpretation of the geometry and kinematics of main faults based on coherence maps, volumetric curvature maps and seismic data. Lower right-hand corner: table showing the maximum horizontal displacement (max. HD) and the type of horizontal displacement in faults F1 to F6. Three families of faults were identified: NE-trending thrusts (yellow), NNW- to N-trending left-lateral strike-slip faults (blue) and WNW- to E-W right- lateral strike-slip faults (green). D) Graph showing the amount and nature of throw (or vertical separation) in three NNW- to N-trending faults (F2 to F4). Throws of faults F2, F3 and F4 were measured every 50 m in their middle part and along their full height. The graph shows a sharp variation in the throw of the faults, and type of vertical offset, providing evidence for horizontal motion. Furthermore, in most faults lateral slip is much larger than vertical (dip) slip.

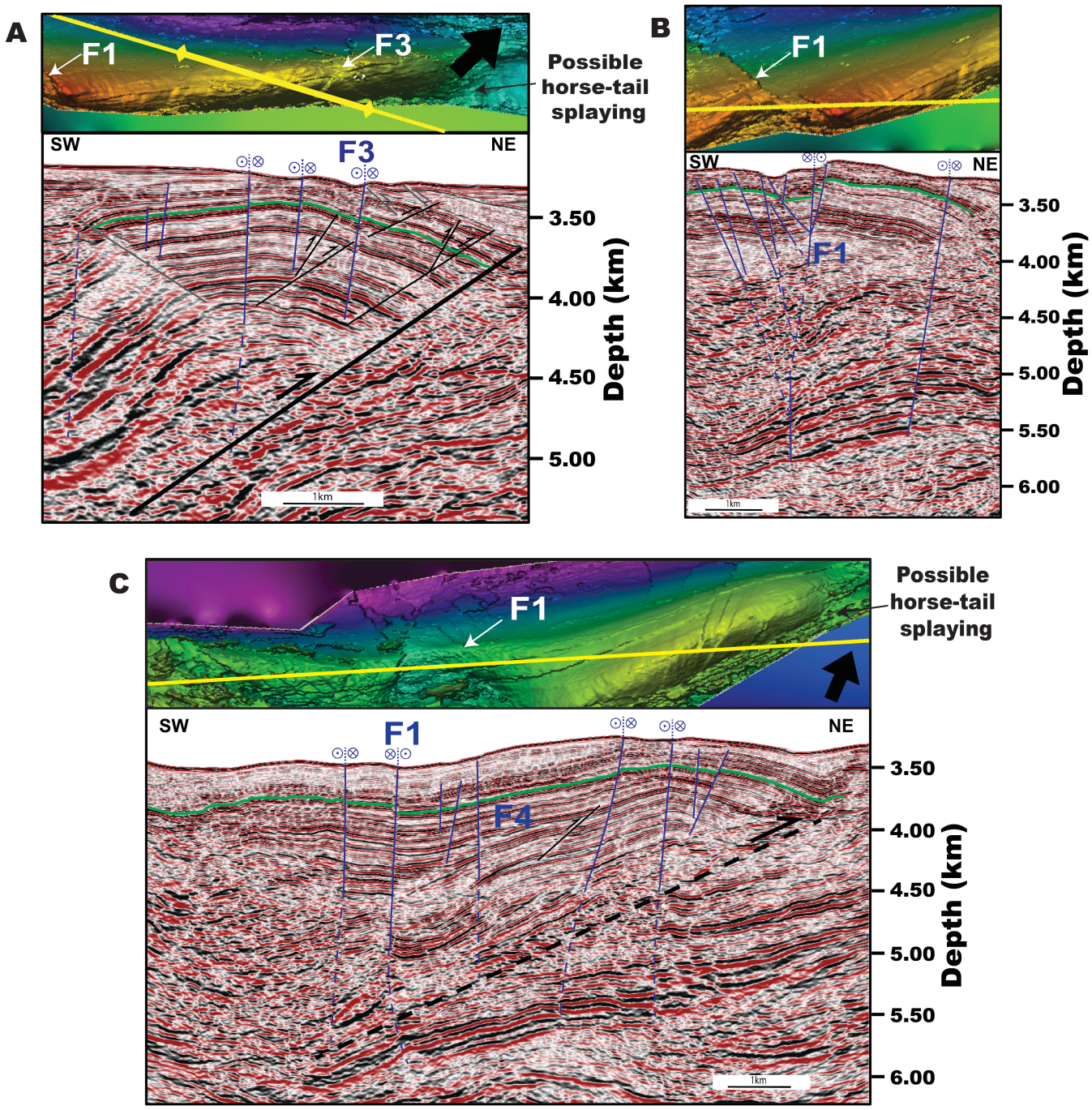

Fig. 4. In this figure, the maps on top show detailed seismic horizons that follow the main thrust anticlines identified in Fig. 3. The seismic profiles below intersect the main thrust anticlines and highlight the geometry of interpreted faults and their kinematics within Unit A. Yellow line - location of the seismic profile below; Green line – seismic horizon of map view above; Blue – strike-slip fault; Black – thrust fault; Grey – antithetic thrust fault. Dashed line – probable fault. A) Seismic crossline 1671. Strike-slip faults intersect and displace primary thrust faults in this profile, whereas larger scale thrusts do not

seem to be affected. B) Seismic crossline 1571. Negative flower structure likely associated with local transtension. C) Seismic crossline 1251. Right-lateral and left-lateral strike-slip faults with variable throws. Some faults are observed on both the hanging-wall and footwall of the thrust anticlines.

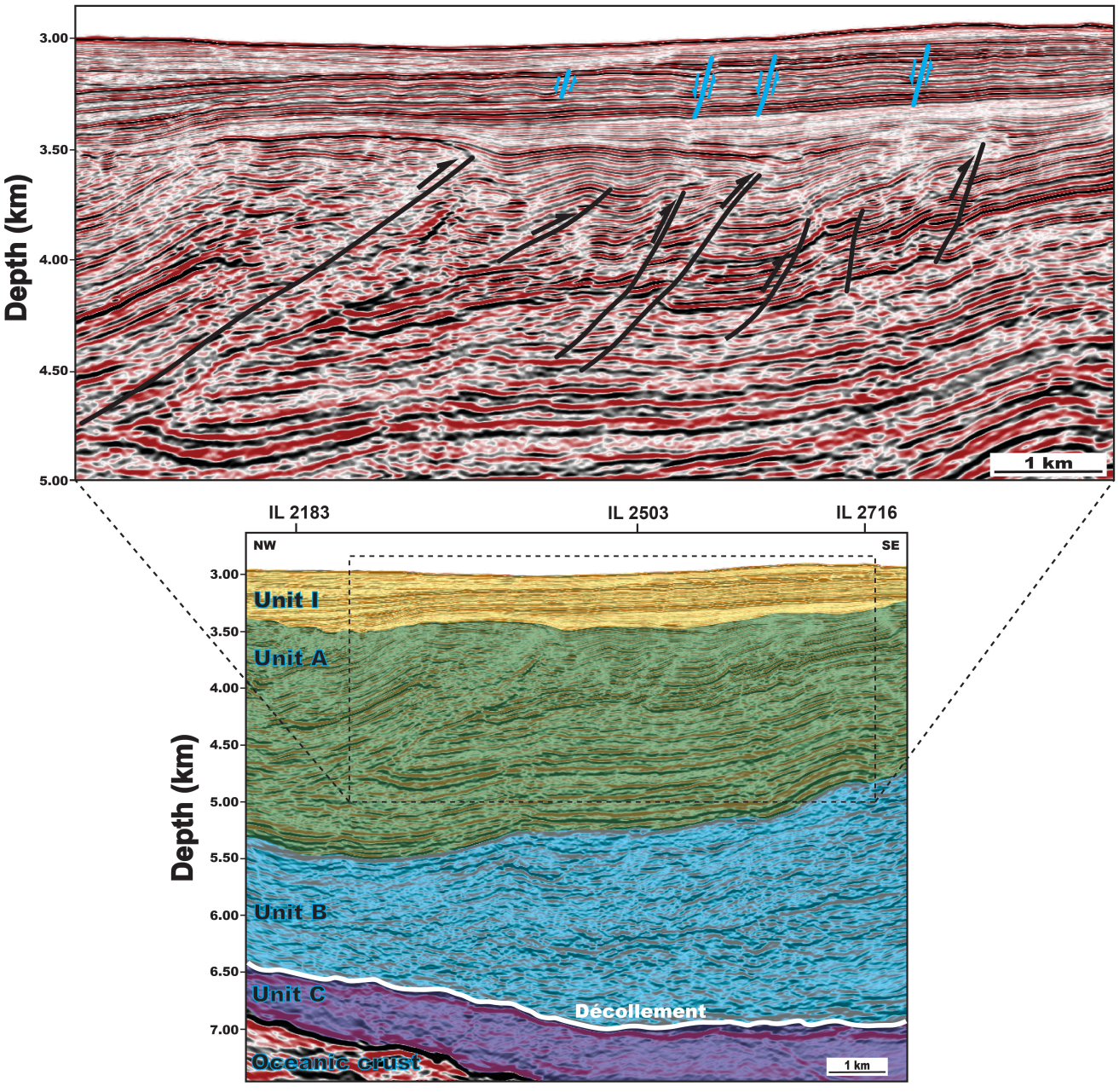

Fig. 5. Depth-migrated seismic profile (crossline 1920) across the landward section of the outer wedge of the NAP showing the tectono-stratigraphic units described in Fig. 2. The inset above shows thrust faults (black lines) within Unit A, where some reach the contact between Units I and A. A few normal faults

(blue lines) within Unit I are associated with the gravitational collapse/stress readjustment that results from local tectonic uplift caused by the deeper thrusts.

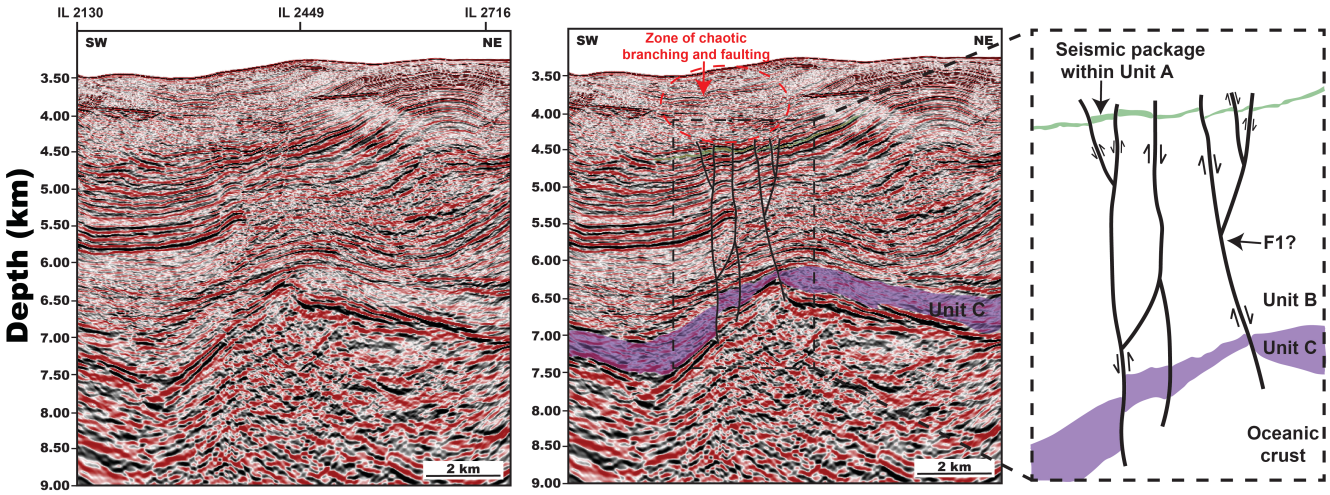

Fig. 6. Depth-migrated seismic profile (crossline 1320; with original profile on the left and interpreted section on the right) showing irregular relative displacements between blocks that are horizontally and vertically adjacent. This disagreement among fault displacements cannot be explained by pure extensional or compressional regimes. Black arrows show the relative displacement between adjacent blocks of strike-slip faults (black lines). Dashed red ellipse highlights a shallower zone of random fractures with minor displacement(s), probably branching from major faults. Some of these minor branches reach the sea floor, affecting the local bathymetry. Green horizon – a seismic horizon of Unit A; Purple horizon – Unit C; IL - Inline

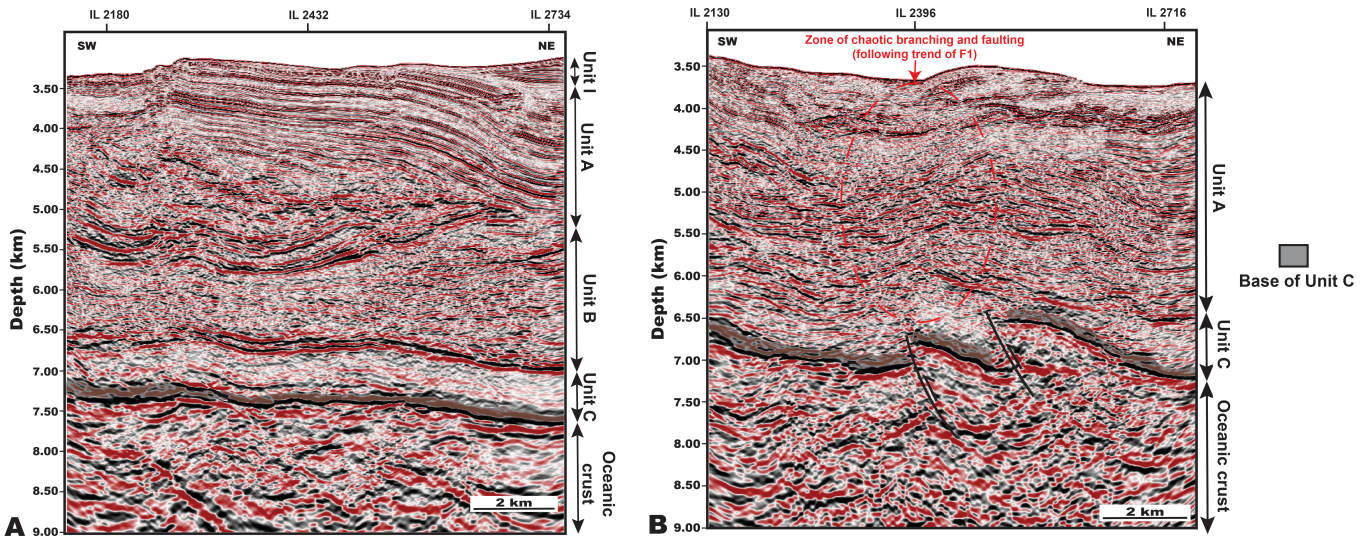

Fig. 7. Depth-migrated crossline 1571 (A) and 1139 (B) showing main tectono-stratigraphic units as described in Fig. 2 and the base of the subduction channel zone (SCZ). A) Unit C and underlying décollement present laterally continuous smooth bases, whereas the overlying Unit A deformed accordingly to the structure described in Fig. 4B. B) Here, both Unit B and the décollement below are folded and displaced by faults that follow the same trend as fault F1. Note the larger structural complexity in Unit A that results from the faults shown in B).

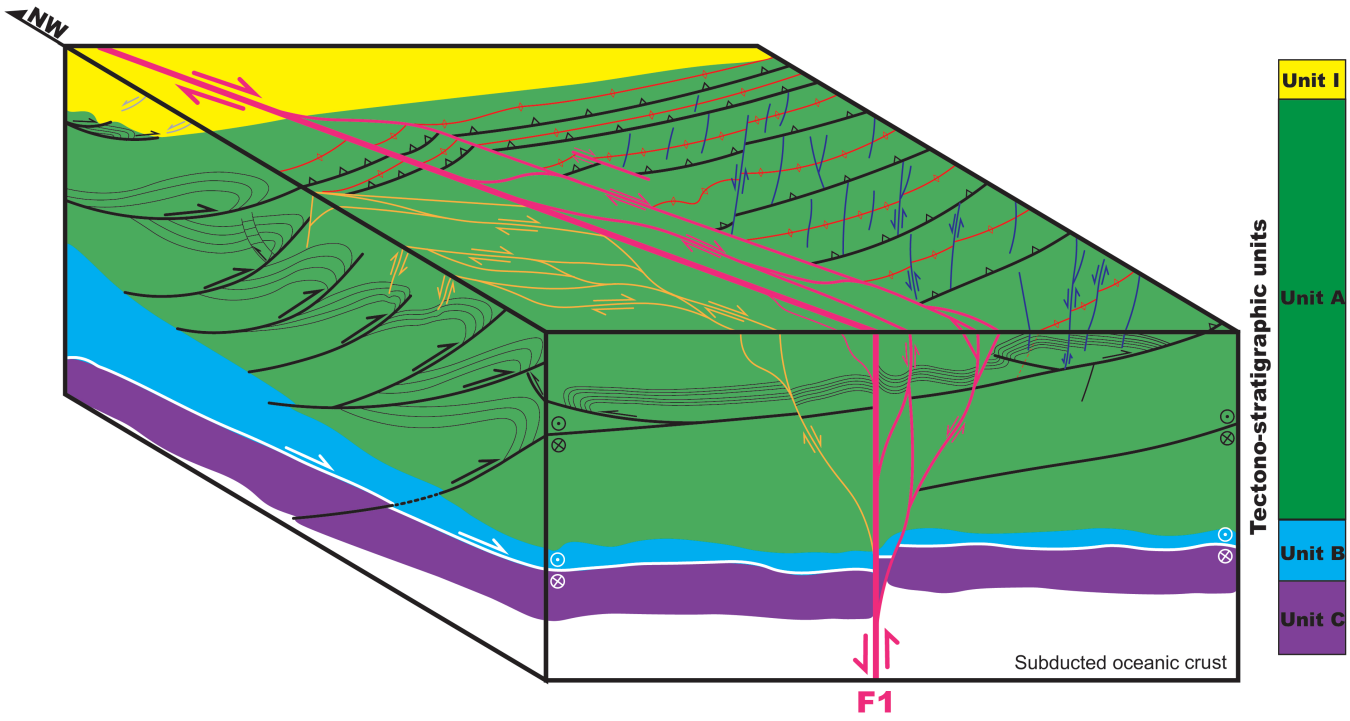

Fig. 8. Schematic block diagram summarising the structural framework of the outer wedge of the NAP (SE of the MSFZ and NW of the FTZ). The figure highlights the observed branching of fault F1 as reflecting a 'flower structure' separating two different structural domains. The NE domain is mainly characterized by well-developed thrust-and-fold structures with left- lateral strike-slip faulting occurring within the major anticlines. The SW domain is characterized by right-lateral strike-slip faults. The relative vertical displacement is not constant in the strike-slip faults within the NAP, meaning these latter are associated with important lateral motion. Red lines – axial planes of thrust anticlines; black lines – synthetic and antithetic thrust faults and corresponding anticlines; pink lines – WNW-trending right-lateral strike-slip faults; orange lines – E-W trending right-lateral faults; blue lines – NNW- to N-trending left-lateral strike-slip faults; grey lines – normal faults in Unit I; white line – décollement fault; half-arrows – relative movement of faults identified on seismic data; pair of circles - relative movement of faults identified on seismic data, where the circle with a dot indicates movement of block toward the reader, and the circle with the cross indicates movement away from the reader.

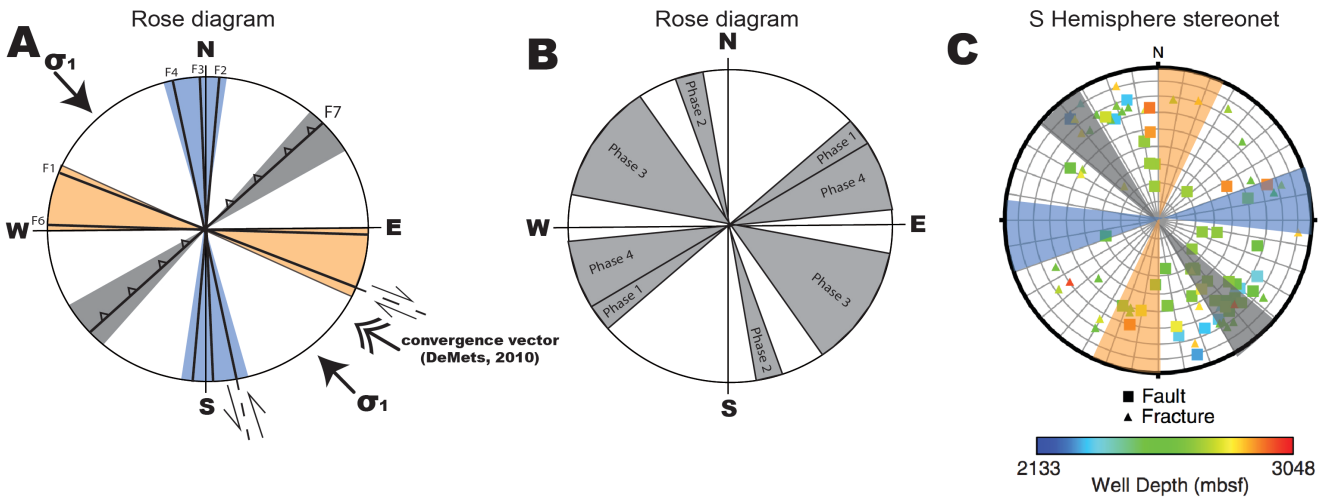

Fig. 9. A) Rose diagram highlighting the range in trends for fault families in the NAP. B) Rose diagram with the trends of each family of normal faults, and their chronological order, according to Moore et al. (2013). C) Lower-hemisphere Schmidt Stereonet with structural data from IODP Site C0002P as analysed in Boston et al. (2016) (note: trends in rose diagrams are rotated 90o from those shown in the stereonets).

left-lateral strike-slip faults. Orange – range of strikes of WNW- to E-W trending right-lateral strike-slip faults.